Insect inspired visual motion sensing and flying robots

Thibaut Raharijaona, Lubin Kerhuel, Julien Serres, Frédéric Roubieu, Fabien Expert, Stéphane Viollet, Franck Ruffier, Nicolas Franceschini

Chapter 1

Insect Inspired Visual Motion Sensing and Bio-Inspired Flying Robots

Thibaut Raharijaona, Lubin Kerhuel, Julien Serres, Frédéric Roubieu, Fabien Expert, Stéphane Viollet, Franck Ruffier and Nicolas Franceschini *

Aix-Marseille University, CNRS, Institute of Movement Science, Biorobotics Department, UMR7287, 13288, Marseille, France

Flying insects excellently master visual motion sensing techniques. They use dedicated motion processing circuits at a low energy and computational costs. Thanks to observations obtained on insect visual guidance, we developed visual motion sensors and bio-inspired autopilots dedicated to flying robots. Optic flow-based visuomotor control systems have been implemented on an increasingly large number of sighted autonomous robots. In this chapter, we present how we designed and constructed local motion sensors and how we implemented bio-inspired visual guidance scheme on-board several micro-aerial vehicles. An hyperacurate sensor in which retinal micro-scanning movements are performed via a small piezo-bender actuator was mounted onto a miniature aerial robot. The OSCAR II robot is able to track a moving target accurately by exploiting the microscanning movement imposed to its eye's retina. We also present two interdependent control schemes driving the eye in robot angular position and the robot's body angular position with respect to a visual target but without any knowledge of the robot's orientation in the global frame. This "steering-by-gazing" control strategy, which is implemented on this lightweight (100 g) miniature sighted aerial robot, demonstrates the effectiveness of this biomimetic visual/inertial heading control strategy.

1. Introduction

Flying insects have been in the business of sensory–motor integration for more than a hundred millions years. These star pilots navigate swiftly through the most unpredictable environments, often attaining a level of agility that greatly outperforms that of both vertebrate animals and present-day aerial robots. Insects are capable of dynamic stabilization, three-dimensional autonomous navigation, ground avoidance, collision avoidance with stationary and nonstationary obstacles, tracking, docking, decking on movable substrates, autonomous takeoff, hovering, landing, and more.

*{thibaut.raharijaona,lubin.kerhuel,julien.serres,frederic.roubieu,fabien.expert,stephane.viollet, franck.ruffier,nicolas.franceschini}@univ-amu.fr

They also behave in a predictive manner, making the appropriate anticipatory postural adjustments that will allow them to take off in the right direction when they notice an approaching threat.[1] Some insects have well-developed learning and memory capacities whose essential mechanisms do not differ drastically from those of vertebrates.[2]

No wonder that insects' neural circuits are highly complex — commensurate with the sophisticated behavior they mediate. However, these circuits can be investigated at the level of single, *uniquely identifiable neurons*, i.e., neurons that can be reliably identified in all the individuals of the species on the basis of their location in the ganglion, their exact shape, and their consistent electrical responses. This great advantage of insect versus vertebrate neuroscience enables insect neuroscientists to accumulate knowledge during anything from a few days to several decades about a given individual neuron or a well-defined neural circuit.[3–5]

This chapter deals with bio-inspired motion sensors and bio-inspired autopilots that may allow robots to fly safely without bumping into things. The chapter first summarizes our attempts to formulate explicit control schemes explaining how insects may navigate *without requiring any distance or speed measurements*. Considering the problem of ground avoidance, we attempted to determine the variables the insect needs to measure, the variables it needs to control, and the causal and dynamic relationships between the sensory and motor variables involved. Inspired by the importance of optic flow in insect behavior,[6] we developed visual motion sensors at our laboratory early in the 1980's.[7–9] With a variety of technological improvements, they became highly miniaturized[10,11] and were more recently installed onboard various aerial prototypes.[11–19] Other groups have developed other types of OF sensors[12–14]and mounted them onboard micro aerial robots.[17,20–23]

Our progress was achieved not only by performing simulation experiments but also by testing our control schemes onboard miniature aerial robots. Constructing a bio-inspired robot first requires exactly formulating the signal-processing principles at work in the animal. After recalling recent advances in the field of optic flow-based autopilots, hyperacuity and bio-inspired optical sensing and gaze stabilization dedicated to aerial robots in section 2 some aspects of the fly visual system are described in section 3. We focus on the realization of fly-inspired OF sensors in section 4. Our aerial robots are based on the use of electronic optic flow sensors[7,8] inspired by the housefly local visual motion sensor, which we previously studied in our laboratory.[24–26] The principle of optic flow regulation is introduced. Visual guidance results are presented in section 5, with applications to aerial vehicles.

Moreover, the property called hyperacuity, which is defined by the ability of a visual system to locate an object with an accuity much greater than the one dictated by the pixel pitch, is discussed in section 6. An hyperacurate optical sensor is presented in section 6.1. Section 7 addresses the problem of implementing an active gaze-stabilization system onboard mobile robots. A complete bio-inspired gaze-control system implemented onboard the OSCAR II robot is described in section

7.

2. Recent advances in the topic

2.1. *Optic flow-based autopilots*

The last decades have provided evidence that flying insects guide themselves visually by processing the *optic flow* (OF) that is generated on their eyes as a consequence of their locomotion. In the animal's reference frame, the translational OF is the *angular speed* ω at which contrasting objects in the environment move past the animal as a consequence of locomotion.[27–31]

Since the early 1990s, several authors have attempted to design and construct bio-inspired flying robots by formulating some of the mechanical and/or signal-processing principles at work in the animal.[14,17,32–37] Among the smallest and lightest flying robots ever built, the project which started in 1998 at University of California, Berkeley, aimed at developing a 25 mm span device capable of sustained autonomous flight. The micromechanical flying insect (MFI) presented in Fig. 1A, was meant to capture some of the exceptional flight performance of true flies.

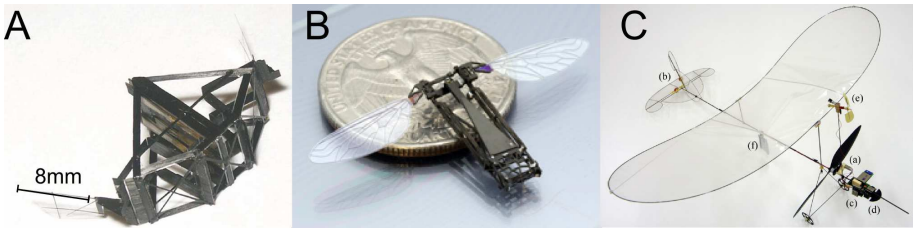

Fig. 1. A: The two carbon wing air frames and the thorax with actuators of the micromechanical flying insect (MFI) from.[38] B: Photograph of the *RoboBee* biologically-inspired two-wing robotic insect[23] C: Autonomous steering of a 10-gram microflyer using an optic flow-based sensor[39] .

Nowadays, Harvard researchers are developing a tethered but controllable micro-air vehicle called Robobee (see Fig. 1B). Recently, the RoboBee has been equipped with optic flow sensors.[23] The MicroCeline robot (see Fig. 1C) is based on a 5-gram living room flyer equipped with a 4mm geared motor and optic flow-based sensor.

Instead of designing an OF-based autopilot for flying robots, evolving neuro controllers have been proliferated and this approach is currently the most popular in evolutionary robotics. Attempts have been made to evolve it in terms of neural controllers by Doncieux[40] and by Zufferey et al.[41]

Recently, the development of effective optic flow-based autopilots present a broad range of challenges and difficulties. The scale of micro aerial vehicles imposes stringent mass and power constraints on all components of the system to allow flight. In,[10,18,20,22,42] the perceived OF is measured on board. In,[43–45] the OF computation is not embedded on the UAV. In,[10,18,33,44] the proposed control approach ensures

optic flow-based terrain following and guarantees that the vehicle does not collide with the ground during the task. In,[45] a nonlinear controller for a vertical take-off and landing (VTOL) unmanned aerial vehicle (see Fig. 2A and B) exploits an OF measurement to control hover above a moving platform and decking on it.

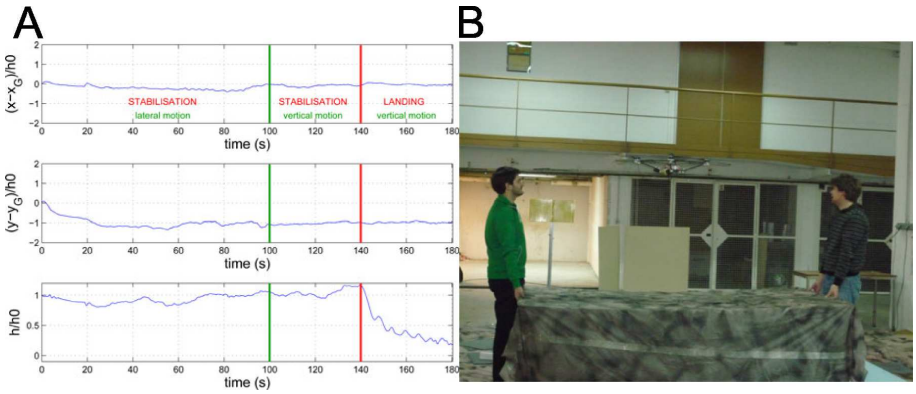

Fig. 2. A: Vertical landing on a moving platform. B: Hovering flight above the landing pad. Figure adapted from.[45]

Light weight UAV (less than 100-gram) have also been equipped with OF sensors.[17,46]

2.2. *Hyperacuity and Bio-inspired optical sensing*

Active vision means that visual perception is not only closely related to the subject's own movements, but that these movements actually contribute to the perceptual processes. For example, invertebrates' eye movements are part of the active visual process used to minimize the adverse rotational optic flow, fixate stationary targets and track moving targets.[47] The small amplitude eye movements (i.e., tremor and micro-saccades) which are known to occur in humans,[48] crabs in,[49] crustaceans in[50,51]and spiders in[52,53] generate temporal changes whose main function is thought to prevent the occurrence of the visual adaptation (fading) which normally occurs when images are perfectly stabilized on the retina.

One of the main advantages of implementing active retinal micro-movements on artificial seeing systems is that they make it possible to detect and locate relevant stationary objects without any need for locomotion. Motion detection plays a major role in visually guided behavior, especially in flying insects, where obstacle avoidance depends on optic flow measurements. Motion detection depends on the measurement of a retinal slip speed (i.e., the optic flow) that is generated by locomotion. However, optic flow can not be the unique sensory modality when hover flight is at stake. By definition, flying in hover with a high accuracy does not allow any motion of the body during a lapse of time. Active retinal micro-movements

allow to perceive without moving (the body) and can even improve the perception beyond the limit imposed by the optics.[54–66]

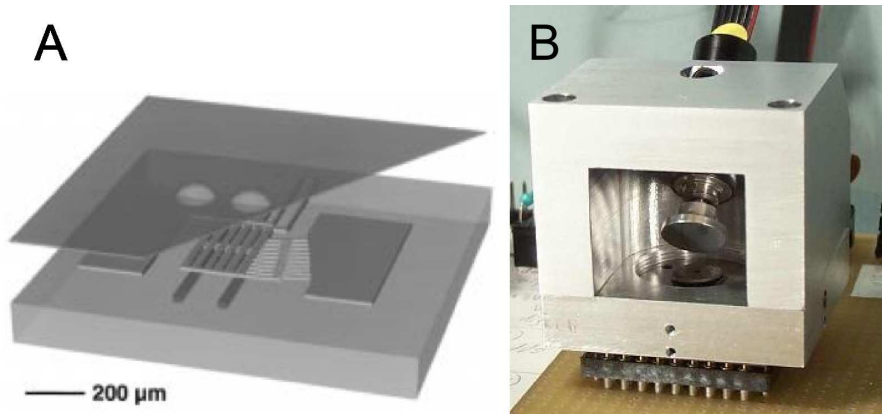

Fig. 3. A: schematic view of the scanning visual sensor. A microlens array is set over a scanning retina, which comprises an electrostatically driven scanning actuator. Adapted from.[59] B: Photograph of the mechanical device producing circular scanning. Adapted from.[67]

Following the first demonstration of the usefulness of retinal microscaning in mobile robotics,[54,55] a micro-sensor was developed that merges sensing and scanning functions on a single-chip by Hoshino et al. (see Fig. 3A). The tiny repetitive translation of the retina produced by the electrostatic scanner generated an effect similar to that of the retinal scanning observed in the housefly compound eyes.[42] In,[67] a new approach to visual sensing for machine vision purposes has been described, which relies on mechanical vibrations in the optical path to turn image features into temporal signals. An integrated circuit implementing a visual sensor taking advantage of this principle has been designed and fabricated (see Fig. 3B).

2.3. *Gaze stabilization for aerial robots*

Ever since animals endowed with visual systems made their first appearance during the Cambrian era, selection pressure led many of these creatures to stabilize their gaze. Navigating in 3-D environments,[68] hovering,[69] tracking mates[70] and intercepting prey[71] are some of the many behavioural feats achieved by flying insects under visual guidance. Recent studies on free-flying flies have shown that these animals are able to keep their gaze fixed in space for at least 200ms at a time, thanks to the extremely fast oculomotor reflexes they have acquired.[72] In vertebrates too, eye movements are also the fastest and most accurate of all the movements. Gaze stabilization is a difficult task to perform for all animals because the eye actuators must be both:

- fast, to compensate for any sudden, untoward disturbances,

- and accurate, because stable visual fixation is required.

In the free-flying fly bee or wasp, an active gaze stabilization mechanism prevents the incoming visual information from being adversely affected by disturbances such as vibrations or body jerks.[72–76] This fine mechanism is way beyond what can be achieved in the field of present-day robotics. The authors of several studies have addressed the problem of incorporating an active gaze stabilization system into mobile robots. A gaze control system in which retinal position measurements are combined with inertial measurements has been developed,[77] and its performance was assessed qualitatively while slow perturbations were being applied by hand. Shibata and Schaal[78] designed a gaze control system based on an inverse model of the mammalian oculomotor plant. This system equipped with a learning network was able to decrease the retinal slip 4-fold when sinusoidal perturbations were applied at moderate frequencies (of up to 0.8Hz). Another adaptive image stabilizer designed to improve the performance of robotic agents was built and its ability to cope with moderate-frequency perturbations (of up to 0.6Hz) was tested.[79] Three other gaze stabilization systems inspired by the human vestibulo-ocular reflex (VOR) have also been presented (two systems for mobile robots[80,81] and one for an artificial rat[82]), but the performance of these systems has not yet been assessed quantitatively on a test-bed. Miyauchi et al have shown the benefits of mounting a compact mechanical image stabilizer onboard a mobile robot moving over rough terrain.[83] Twombly et al. have carried out simulations on a neuro-vestibular control system designed to endow a walking robot with active image stabilization abilities.[84] In the humanoid research field, some robotic developments have addressed the need to stabilize the gaze by providing robots with visuo-inertial oculomotor reflexes (e.g.:[85–88]). Wagner et al. built a fast responding oculomotor system,[89] using air bearings and bulky galvanometers. An adaptive gaze stabilization controller was recently described, but the performances of this device were measured only in the 0.5-2Hz frequency range.[90] Recently, Maini et al. succeeded in implementing fast gaze shifts on an anthropomorphic head but without using any inertial-based oculomotor reflexes.[91] None of the technological solutions ever proposed so far are compatible, however, with the stringent constraints actually imposed on miniature aerial robots.

The gaze stabilization mechanisms of flying insects such as flies, are based on fine oculomotor reflexes that provide the key to heading stabilization. These high performance reflexes are of particular relevance to designing tomorrow's fast autonomous terrestrial, aerial, underwater and space vehicles. As we will see, visually mediated heading stabilization systems require:

- a mechanical decoupling between the eye and the body, (either via a neck, as in the fly compound eye, or via the orbit, as in the vertebrate's "camera eye")
- an active coupling between the robot's heading and its gaze, via oculomotor reflexes

- a fast and accurate actuator. Flies control their gaze using no less than 23 pairs of micro-muscles[3]
- a visual fixation reflex (VFR) that holds the gaze steadily on the target.
- a vestibulo-ocular reflex (VOR), i.e., an active inertial reflex that rotates the eye in counter phase with the head. Flies typically use an inertial reflex of this kind which is based on the halteres gyroscopic organ, especially when performing roll movements.[73] A similar system was also developed in mammals – including humans - some hundred million years later. Rhesus monkeys' VORs are triggered in the 0.5-5Hz[92] and even 5-25Hz[93] frequency range, and are therefore capable of higher performances than humans.
- a proprioceptive sensor which is able to measure the angular position of the eye in the head or in the body. Although the question as to whether this sensor exists in the primate oculomotor system is still giving rise to some controversy,[94,95] it certainly exists in flies in the form of a pair of mechanosensitive hair fields located in the neck region.[96] The latter serves to measure and compensate for any head-body angular deviations in terms of pitch,[72] roll[73] and yaw.[97]

The study presented in this chapter was inspired by insects' and vertebrates' oculomotor systems, our quest was primarily for the performance.

3. The fly's eye

Flies are agile seeing creatures that navigate swiftly through the most unpredictable environments, avoiding all obstacles with little conventional aerospace avionics. Equipped with "only" about one million neurons and "only" 3000 pixels in each eye, the housefly, for example, achieves e.g., 3D navigation and obstacle avoidance at an impressive 700 body-lengths per second. All this is achieved, surprisingly, without any connections of the animal to a super-computer and an external power supply. The impressive lightness of the processing system at work onboard a fly or a bee makes any roboticist turn pale once he/she realizes that these creatures achieve many of the behaviours that have been sought for in the field of autonomous robotics for the last 50 years: dynamic stabilization, 3D collision avoidance, tracking, docking, autonomous landing, etc.

The front end of the fly visual system consists of a mosaic of facet lenslets (see foreground in Fig. 4) and an underlying layer of photorececeptor cells forming the retina proper (see background in Fig. 4). The photoreceptor cells are more sensitive and reliable than any photomultiplier ever built. In addition, flies possess one of the most complex and best organized retinas in the animal kingdom.

In the mid 1980's, we started designing a robot to demonstrate how an agent could possibly navigate in a complex environment on the basis of optic flow. The robot was equipped with a planar, curved compound eye driving an array of fly-inspired Elementary Motion Detectors.[26]

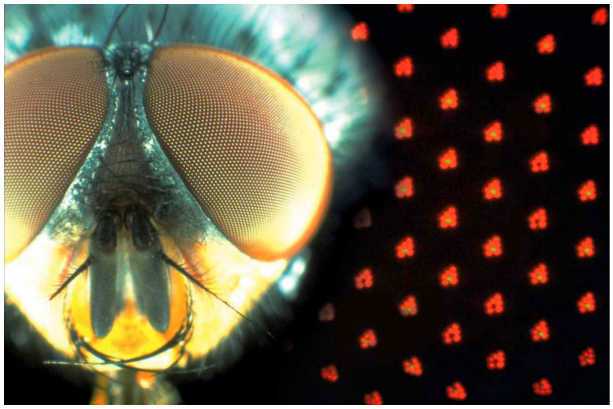

Fig. 4. Head of the blowfly Calliphora erythrocephala (male) showing the two panoramic compound eyes with their facetted cornea (foreground). Each facet lens is the front-end of an ommatidium that contains a small group of photoreceptor cells (background). There are as many sampling directions (pixels) in each eye as there are facets. This photograph was taken with a custom-made Lieberkühn microscope based on two parabolic mirrors extracted from bicycle lights . Figure from.[98]

The latter was used to sense the OF generated by the robot's own locomotion among stationary objects. The 50-cm high ''robot-mouche" (Robot-Fly in English) that we realized in 1991 (see Fig. 5A) was the first OF-based, completely autonomous robot able to avoid contrasting obstacles encountered on its way, while traveling to its target at a relatively high speed (50 cm/s).[26,99–101] The Robot-Fly was also based on ethological findings on real flies, whose most common flight trajectories were shown to consist of straight flight sequences interspersed with rapid turns termed saccades.[6,68,103–105]

Based on the findings obtained at our Laboratory on the fly's visual sensory system,[25] several versions of the 2-pixel Local Motion Sensor (LMS)[11,16,26,106,107] were developed, using an algorithm introduced by,[7,9] which was later called the "time of travel scheme" (see[108–110]). Other vision-based systems were more recently designed to measure the optic flow onboard UAVs (Unmanned Aerial Vehicles).[17,111–115] Most of these visual systems were quite demanding in terms of their computational requirements and/or their weight or were not very well characterized, except for the optical mouse sensors,[21] with which a standard error of approximately $\pm 5^\circ/s$ around $25^\circ/s$ was obtained in a $\pm 280^\circ/s$ overall range. More recently we developed at the laboratory the concept of Visual Motion Sensor (VMS) fusing the local measurement from several 2-pixel LMS to measurement the 1-D optic flow more accurately and more frequently.[116–119]

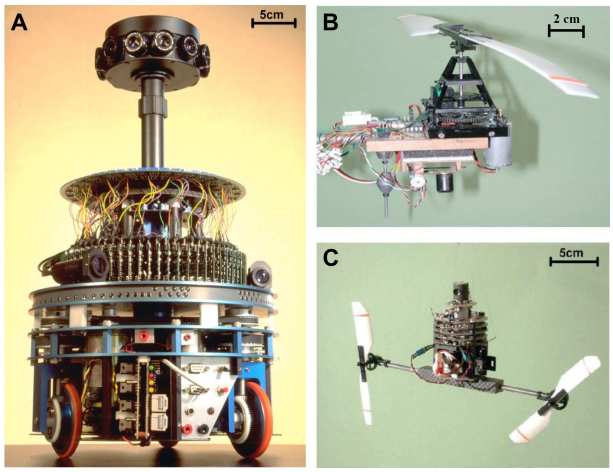

Fig. 5. Three of the visually-guided robots designed and constructed at the Laboratory on the basis of our biological findings on visuomotor control in flies. (A) The Robot-Fly ("robot-mouche" in French) incorporates the compound eye (visible at half-height) for obstacle avoidance, and a dorsal eye for detecting the light source serving as a goal. This robot (height: 50 cm; weight: 12 kg) reacts to the optic flow generated by its own locomotion amongst obstacles.[26,99–101] It is fully autonomous as regards its processing and power resources. (B) The robot OCTAVE (Optic flow-based Control sysTem for Aerial VEhicles) is a 100-gram rotorcraft equipped with a 2-pixel ventral eye sensing the OF on the terrain below. This self-sustained aerial creature is tethered to a light rotating arm that allows only three degrees of freedom: forward and upward motion and pitch. The robot lifts itself and circles around a central pole at speeds up to 3 m/s. It ascends or descends depending on the ventral optic flow it measures.[10,18,37] (C) The robot OSCAR (Optic flow based Scanning sensor for the Control of Aerial Robots) is a 100-gram, twin-engined aircraft equipped with a two-pixel frontal visual system that relies on visual motion detection and on a microscanning process inspired by the fly.[42] It is tethered to a 2-meter-long nylon wire secured to the ceiling of the laboratory. Vision and rate gyro signals combine onboard to make OSCAR fixate and track a target (a dark edge or a bar) with hyperacuity at speeds of up to 30°/s.[57] Figure from.[102]

4. Insect-based visual motion sensors

Many methods of measuring the visual angular speed have been used for robotic purposes, such as those involving the local 1-D Hassenstein and Reichardt correlator scheme.[120] Some motion sensors of this type have been mounted on terrestrial robots.[121,122] The interpolation image algorithm (I2A)[123] combined with a 1-D camera array have been used onboard an indoor microflyer.[46] The "time of travel" scheme[7] combined with off-the-shelf photodiodes has been implemented on both terrestrial robots[26,54] and tethered flying robots.[10,18,33,60]

In addition, some indoor terrestrial robots[124] have been equipped with standard cameras combined with navigation systems based on OF principles.[125] Off-the-shelf computer mouse sensors measuring local 2-D optic flow were recently characterized[126,127] and mounted onboard terrestrial[128,129] and aerial[20,112] robotic platforms navigating under constant lighting conditions.

Other visual motion sensors have been developed using analog and digital Very-Large-Scale Integration (VLSI) technologies (see[13,130–132] for 1-D motion sensors;[109,133] and in the case of 2-D optic flow sensors). Some other bio-inspired VLSI sensors based on the use of optic flow cues have been developed for collision detection purposes.[134]

However, to our knowledge, very few robotic studies have been published so far in which visual motion sensors have been implemented and tested outdoors, where the illuminance cannot be easily controlled (see[13,107] for linear 1-D motion sensors, and see[20,43,112,135] for 2-D optic flow sensors).

Although visual motion sensors are of great interest for robotic applications, very few attempts have been made so far to characterize systems of this kind. Some authors have tested their visual motion sensors with virtual objects presented on a video screen (using a 1-D local motion sensor[110] or 2-D optic flow sensors[136]) and the performance of some VLSI motion sensors has been described in detail (see,[121,131] for a 1-D motion sensor characterized indoors and in front of photographs of natural scenes, respectively).

It therefore seemed to be worth developing means of testing the reliability of the visual motion sensors developed at our laboratory in terms of their resolution, accuracy, sensitivity, and invariance to contrast in real environments under a large range of illuminance values. In this section, it was proposed to present two custom-made, bio-inspired 1-D local motion sensors[137] based on a two-pixel system with different front ends, namely,

1. the APIS (adaptive pixels for insect-based sensors)-based local motion sensor[107,117,137]involving the use of a custom-made VLSI array equipped with Delbrück-type auto-adaptive pixels, and

2. the LSC-based local motion sensor[107,138,139] involving the use of off-the-shelf linearly amplified photosensors (the LSC component was purchased from iC-Haus) each of which is equipped with an onchip preamplification stage.

Our visual motion scheme processes the time elapsing between the detection of any contrasting feature by two adjacent photoreceptors.[7,11,26,99,140] This scheme was originally inspired the results of electrophysiological studies on the housefly's visual system, where single elementary motion detector neurons (EMDs) were optically stimulated.[141] The EMD response was picked up from the H1 neuron, one of the 60 Lobula Plate tangential cells (LPTCs). The local motion processing scheme inspired by these studies[9] belongs to the token-matching schemes[142] and has been called the "time of travel" scheme.[110,143] In the mid-1990s, a similar principle was used again to design a smart VLSI circuit called the "facilitate and sample" sensor.[108]

The characteristics of the two local motion sensors in question were determined here by recording their responses to a purely rotational optic flow generated by rotating the sensors mechanically indoors and outdoors. In the case of a stationary environment, the rotational optic flow ω, which is by definition independent of the

distance from the sensors to the surrounding objects,[144] can be directly compared to the rate gyro output signal denoted Ω_{gyro}.

4.1. *Description of the local visual motion sensors*

Basically, each of the APIS-based and LSC-based visual motion sensors consists of a lens placed in front of a photosensor array: each visual motion sensor processes the output signals generated by two photodiodes.

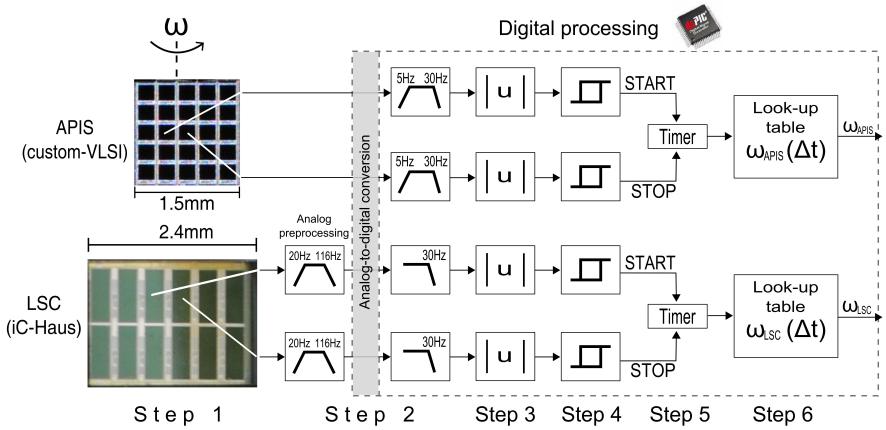

Fig. 6. General processing architecture of the APIS-based and LSC-based local motion sensors. In each sensor, the output signals emitted by two adjacent pixels were spatially and temporally filtered and thresholded to determine the angular speed ω. The "time of travel" scheme previously developed at Franceschini's laboratory[7,140] was used to measure the local visual motion. The angular speed measured by each sensor ω_{meas} is the ratio between the constant interreceptor angle ϕ and the time t elapsing between the first and second thresholded signals. The overall processing of the two local motion sensors was carried out in parallel on the same microcontroller (dsPIC 33FJ128GP804) at a sampling frequency of 2 kHz. In the case of the LSC-based motion sensor, the two photodiode outputs were first filtered by an analog band-pass filter with cutoff frequencies (20, 116 Hz) before being filtered by a digital second-order, low-pass filter with a cutoff frequency of 30 Hz. In the case of the APIS-based motion sensor, the two photodiode outputs were filtered by a digital band-pass filter with cutoff frequencies (5,30 Hz). Figure from[107]

Each photodiode's output signal is transmitted to a processing unit, where a digital version of the visual motion algorithm assesses the relative angular speed ω of any contrasting features encountered in the environment (see Fig. 6) (i.e., a 1-D component of the optic flow). In this paragraph, 2 two-pixel motion sensors based on the same "time of travel" principle but equipped with two different front ends were presented (see Fig. 7).

The front end of the APIS-based local motion sensor was based on adaptive pixels, originally suggested by.[145] The whole APIS (adaptive pixels for insect-based sensors) retina, a custom-made VLSI retina comprising 25 pixels (see Figure 7(d)), was developed in collaboration with the Center for Particle Physics (CPPM)

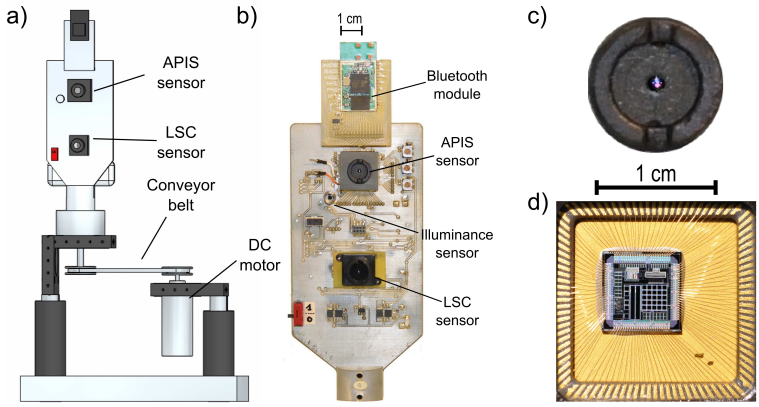

Fig. 7. Test board that includes both local motion sensors. (a) Sketch of the full mechanical system. A mechanical rotational angular speed was imposed on the board by means of a dc motor (2233012S from Minimotor) regulated via a proportional-integral controller. (b) Picture of the sensor board, which included the two custom-made visual motion sensors, an illuminance sensor based on a single elementary photodiode, and on the other side of the board (not visible here), a rate gyro (Analog Devices; ADIS 16100) measuring the reference mechanical angular speed (i.e., the rotational speed of the board) and a 16-bit microcontroller (dsPIC 33FJ128GP804) equipped with several 12-bit ADC (analog to digital converter) inputs. The microcontroller processes the visual signals received by the two visual motion sensors at a sampling frequency of 2 kHz. The measured visual motion ω_{meas} and the rotational speed gyro are recorded synchronously and sent to a computer via a Bluetooth module connected to a small battery (LiPo, 300 mAh-3.3 V). This wireless link leaves the sensor board free to rotate autonomously. (c) The visual motion sensors' miniature camera lens (Sparkfun SEN-00637, focal length 2 mm, f-number 2.8) is defocused with respect to the focal plane to create a Gaussian angular sensitivity. (d) The APIS sensor along with the 5×5 photodiode array and an auto-adaptive circuit: only two pixels are connected to the dsPIC microcontroller.Figure from[107]

in Marseilles.[137,146] Each pixel features an integrated photodiode with a sensitive area of 250×250 μm connected to an adaptive, time-continuous, logarithmic circuit having a dynamic range of 100 dB.

The front end of the LSC-based local motion sensor was based on an off-the-shelf photodiode array (LSC is a component purchased from iC-Haus) consisting of two rows of six pixels. To make the sensor able to distinguish a larger number of contrasting patterns at low illuminance levels, we summed the two pixels in the same column to improve the signal-to-noise ratio by increasing the sensitive area to 300×1600 μm. These two "elongated photosensors" were combined with a classical fixed-gain photocurrent amplifier implemented using surface mount device (SMD) components.

The original local motion detector[7,11,140] (also called "time of travel") consisted of an analog circuit producing an output signal that increased as the time lag t between its two inputs decreased. The out-put signal therefore increased with the angular speed ω. Like the fly's motion-detecting neurons by which it was originally inspired (Franceschini et al., 1989), our visual motion sensors can react to

either dark-to-light (ON) or light-to-dark (OFF) contrasts. The bio-inspired signal processing method implemented in each of the two local motion sensors can be decomposed into six steps[7,11,140] (see Fig. 6) as follows:

- Step 1: Spatial sampling and low-pass spatial filtering (which is achieved by defocusing the miniature camera lens to obtain a Gaussian angular sensitivity for each pixel),
- Step 2: Band-pass temporal filtering: high-pass temporal filtering to differentiate the visual signals and low-pass temporal filtering to reduce the noise such as the 100-Hz interference originating from artificial lighting (this step is partially analog in the case of the LSC-based visual motion sensor),
- Step 3: Taking the absolute value of the signals to detect both dark-to-light and light-to-dark contrast transitions,
- Step 4: Thresholding with fixed values regardless of the illuminance background,
- Step 5: Measuring the time Δt (time of travel) elapsing between the thresholded signals,
- Step 6 : Computing the local angular speed by applying the ratio between the interreceptor angle $\Delta\varphi$ and the time elapsing Δt between the moments when two adjacent photodiode signals reach the threshold (i.e., the time of travel of a contrast from the optical axis of one photodiode to the optical axis of the following one),

$$\omega_{meas} = \frac{\Delta\varphi}{\Delta t} \tag{1}$$

This overall processing was carried out on a dsPIC33FJ128GP804 microcontroller working at a sampling frequency of 2 kHz in floating-point arithmetic. The overall signal processing tasks do not require performing any time-consuming tasks such as division be-cause a look-up table was used to transform the tinto the visually perceived angular speed ω_{meas} [see Eq. (1)]. All embedded algorithms were developed on Matlab with a Simulink blockset for dsPIC called Embedded Target for dsPIC.

5. Optic-flow regulation for guidance and navigation

5.1. *The problem of ground avoidance*

To control an aircraft, it has been deemed essential to measure state variables such as ground height, ground speed, descent speed, etc. The sensors developed for this purpose (usually emissive sensors such as radio-altimeters, laser rangefinders, Doppler radars, GPS receivers, forward-looking infrared sensors, etc.) are far too cumbersome for insects or even birds to carry and to power. The OF sensors

evolved by natural flyers over the last few hundred million years are at odds with these avionic sensors. OF sensors are *nonemissive* sensors.

The ventral OF experienced in the vertical plane by flying creatures — including aircraft pilots — is the relative angular velocity ω generated by a point directly below on the flight track.[28,147] As shown in Figure 8A , the translational OF perceived vertically downward depends on both the ground speed V_x and the ground height h and is equal to the ratio between these two variables:

$$\omega = {}^{V_x}/_{h}[rad.s^{-1}] \tag{2}$$

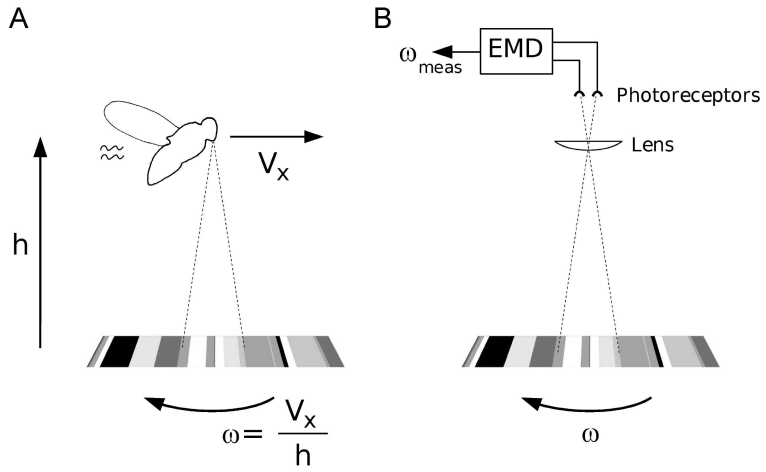

Fig. 8. A: Definition and measurement of the ventral optic flow ω experienced by an insect (or a robot) flying in translation in the vertical plane. B: An EMD like the EMDs driving the honeybees' VT neurons,[148] is able to measure the ventral OF (i.e., the angular speed ω at which any contrasting feature moves under the flying agent). Figure from.[106]

We know that flies and bees are able to react to the translational OF, ω independently of the spatial texture and contrast.[149,150] We also know that some of their visual neurons may be involved in this reaction because they respond monotonically to ω with little dependence on texture and contrast.[148] Neurons facing downward can therefore act as ventral OF sensors, and thus assess the V_x/h ratio (Fig. 8).

Based on laboratory experiments on mosquitoes and field experiments on locusts, Kennedy put forward an hypothesis, according to which flying insects maintain a "preferred retinal velocity" with respect to the ground below.[27,29] In response to wind, for example, insects may adjust their ground speed or ground height to restore the apparent velocity of the ground features. Kennedy's hypothesis has been repeatedly confirmed during the last 30 years: both flies and bees were found to maintain a constant OF with respect to the ground while cruising or landing,[151–153] except in *Drosophila*.[154]

The problem is how insects may achieve this feat, since maintaining a given OF is a kind of chicken-and-egg problem, as illustrated by Eq. 2. An insect may hold its ventral OF, ω constant by adjusting either its ground speed (if it knows its ground height) or its ground height (if it knows its ground speed). In addition, the insect could maintain an OF of 1 rad/s (i.e., 57 degrees/s), for instance, by flying at a speed of 1 m/s at a height of 1 meter or by flying at a speed of 2 m/s at a height of 2m. An infinitely large number of possible combinations of ground speed and ground height will give rise to the same "preferred OF".

Drawing on the experience we had with OF-based visual navigation of a terrestrial robot,[9,26] we attempted early to develop an explicit flight-control scheme for aerial navigation in the vertical plane. Our first tentative step on these lines was not particularly successful, because we were cornered in the general notion that prevailed in those days that insect navigation relies on gauging range.[26,149] In the experimental simulations we performed in 1994, for example,[32] we assumed that the insect (or the robot) would know its ground speedV_x (by whatever means), so that by measuring it would be able to gauge the distance h from the ground (Eq. 2) and react accordingly to avoid it. Although this procedure is still used in robotics (see, e.g.,[43,155]), where ground speed can be determined (e.g., via GPS), this makes the way insects operate all the more elusive.

5.2. *The optic flow regulation principle*

In spite of this early success to explain how an insect could navigate on an OF basis, we considered that Kennedy's insightful hypothesis was calling for a clear formalization that would bring to light:

- The flight variables really involved,
- The sensors really required,
- The dynamics of the various system components,
- The causal and dynamic links existing between the sensory output(s) and the variable(s) to be controlled,
- The point of application of the various disturbances that an insect will experience in fl ight and the variables it will have to control to compensate for these disturbances.

We came up with an autopilot called OCTAVE (Optical altitude Control sysTem for Autonomous VEhicles) that is little demanding in terms of neural (or electronic) implementation and could be just as appropriate for insects as it would be for aircraft.[10] A ventral OF sensor was integrated into a feedback loop that would drive the robot's lift, and thus the ground height, so as to compensate for any deviations of the OF sensor's output from a given set point.[10,18,37,106] As we will see, this simple autopilot (Fig. 9A) enabled a micro-helicopter to perform challenging tasks such as take-off, terrain following, reacting suitably to wind, and landing.

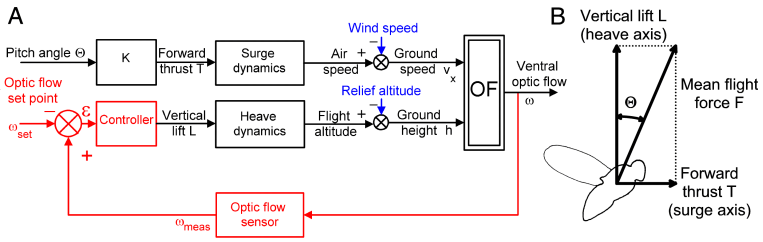

Fig. 9. A: The OCTAVE optic flow regulator (bottom feedback loop) controls the mean flight force vector and hence the lift, and hence the ground height, so as to maintain the ventral optic flow ω constant and equal to the set-point ω_{set}. B: Flies, like helicopters, pitch forward slightly to increase their forward thrust, and hence their airspeed. As long as they pitch forward by $\Theta < 10°$, the lift component L does not incur any major loss. Figure from[106]

The OCTAVE autopilot can be said to be an OF regulator. The word *regulator* is used here as in control theory to denote a *feedback control system* designed to maintain an output signal constantly equal to a given set point. The Watt fly-ball governor from the 18th century, for instance, was not only one of the first servomechanisms ever built: it was also the very first angular speed regulator. It served to maintain the rotational speed of a steam engine shaft at a given set point, whatever interferences occurred as the result of unpredictable load disturbances. The Watt regulator was based on a rotational speed sensor (meshed to the output shaft), whereas the OF regulator is based on a noncontact rotational speed sensor — an OF sensor — that measures the ventral OF (again in rad/s).

Specifically, the OF signal ω_{meas} delivered by the OF sensor (see Fig. 9A) is compared with the OF set point, ω_{set}. The comparator produces an error signal: $\epsilon = \omega_{meas} - \omega_{set}$ which drives a controller adjusting the lift L, and thus the ground height h, so as to minimize ϵ. All the operator does is set the pitch angle Θ and therefore the airspeed (see Figure 9A). The OF regulator does the rest: that is, it attempts to keep ω constant by adjusting the ground height h proportionally to the current ground speed V_x.

5.3. *A micro-helicopter equipped with an OF sensor and an OF regulator*

We tested the idea that insects may be equipped with a similar OF regulator by comparing the behavior of insects with that of a "seeing helicopter" placed in similar situations. The OCTAVE robot we built (Fig. 10A) is a micro-helicopter equipped with a simple, two-pixel ventral eye driving an EMD acting as an OF sensor (Fig. 10A).

Any increase in the rotor speed causes the OCTAVE aerial robot to rise, and the slightest (operator-mediated) forward ("nose-down") tilting by a few degrees produces a forward thrust component that causes the MH to gain forward speed. The flight mill is equipped with ground-truth azimuthal and elevation sensors that

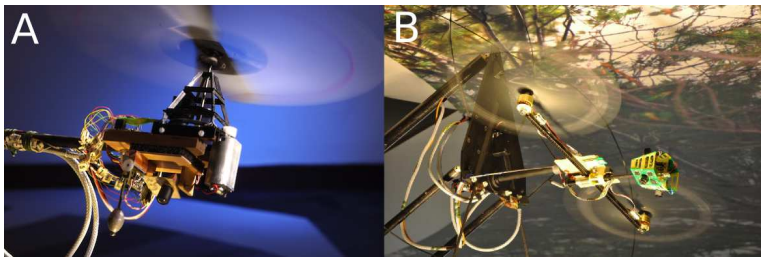

Fig. 10. A: 100-gram micro-helicopter (OCTAVE robot) equipped with a ventral OF sensor and the OF regulator. The aerial robot can be remotely pitched forward by a small angle Θ while keeping its roll attitude. The flight mill is equipped with ground-truth azimuthal and elevation sensors with which the position and speed of the OCTAVE robot can be monitored accurately in real time. Picture from[18] B: The robot called BeeRotor is a tandem rotorcraft that mimicks optic flow-based behaviors previously observed in flies and bees .Picture from[138]

allow the position and speed of the OCTAVE aerial robot to be monitored at high accuracy and in real time. Since the OCTAVE purpose was to demonstrate a basic principle, it was equipped with an elementary ventral eye composed of only two photoreceptors driving a single EMD as shown in.[10]

More recently, we built a miniature robot (80g) called Beerotor,[138] which is autonomous in terms of its computational power requirements. Beerotor is equipped with a 13.5-g quasi-panoramic visual system (Fig. 10B) and regulates its optic flow with respect to the ceiling or the ground to control both its speed and altitude.

Vertical Optic flow regulation enable autonomous aerial robots (such as OCTAVE and Beerotor) to perform 4 further reputedly difficult tasks: autonomous take off, autonomous terrain following, autonomous landing and autonomous compensation for wind disturbances.

5.4. *Micro-hovercraft against honeybees' behavioral patterns*

Behavioral experiments on several insect species have long shown that motion perceived by the lateral part of their compound eyes affects the forward thrust, and hence the forward speed (for review, see[106]). First, when flying through a tapered corridor, honeybees slowed down as they approached the narrowest section and speeded up when the corridor widened beyond this point.[151] The authors concluded that bees tended to adjust their speed proportionally to the local corridor width by regulating the image velocity. Second, when flying through a straight corridor, honeybees tended to fly along the midline.[149] To explain this "centering behavior," the authors hypothesized that bees were balancing the speeds of the retinal images (i.e., the lateral OFs) of the two walls, a hypothesis that subsequently gave rise to many wheeled and aerial robots capable of centering in a corridor (e.g.,[124]).

We recently found, however, that honeybees trained to fly along a larger corridor do not systematically center on the corridor midline (Fig. 11B,C). They keep remarkably close to one wall, even when part of the opposite wall is missing

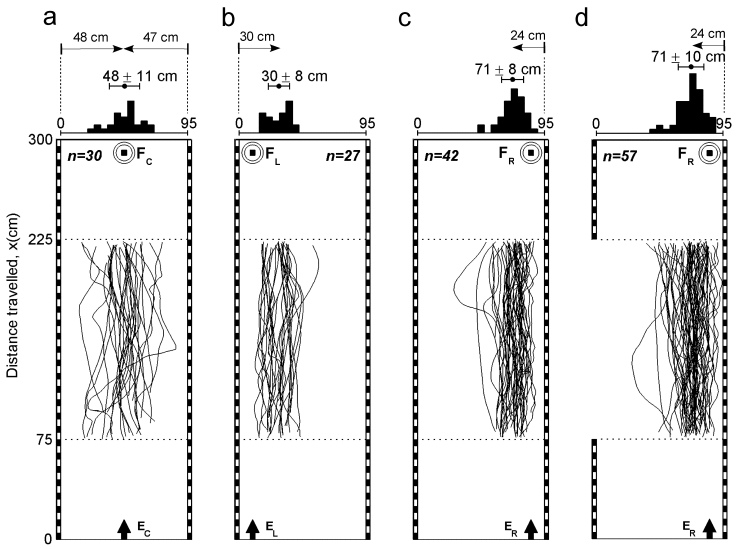

Fig. 11. Honeybees' *centering* and *wall-following* behaviors. Bees were trained to enter a wide (width 0.95 m) 3-meter long corridor, formed by two 0.25-m high walls lined with vertical white-and-gray stripes (period 0.1m; contrast $m = 0.41$). The bee's entrance (E_C) and the feeder (F_C) were placed either on the corridor midline (a) or on one side (b, c, d). In (d), part of the left wall was removed during the trials. Mean distances distribution as shown on top. From.[156]

(Fig. 11D). Distance from that wall (D_R or D_L) and forward speed V_x were, on average, such that the speed-to-distance ratio (i.e., the lateral OF) was maintained practically constant, at about 230°/s in our 95cm wide corridor.[156]

With a view to explaining the various honeybee behaviors observed in the various corridors, we came up with the design of the LORA III autopilot (LORA III stands for Lateral Optic flow Regulator Autopilot, mark III), which is able to control both the forward speed V_x of the vehicle and its lateral distances D_R and D_L from the two corridor walls jointly, without *ever measuring any speeds or distances* (Fig. 12A).

Our sighted LORA robot is a retro-fitted version of a miniature RC hovercraft (Taiyo Toy LtD, Typhoon T-3). The miniature LORA robot (mass: 0.878kg, size: 0.36x0.21x0.17m, see Fig. 12B) is fully actuated by means of four ducted fans (GWS EDF-50, DC motor CN12-RLC, mass: 30g) driving it on the horizontal plane. The two rear thrusters actuate the robot along the surge axis, the two lateral thrusters actuate the robot along the sway axis, and the robot's heading is adjusted by controlling the two rear thrusters differentially. An additional lift fan (a brushless motor Micro Rex 220/3-3200 Flyware fan, mass: 11g) inflates the skirt to create an air-cushion preventing the robot from touching the ground. The vehicle is naturally stable in terms of the pitch and roll and the very low friction coefficient

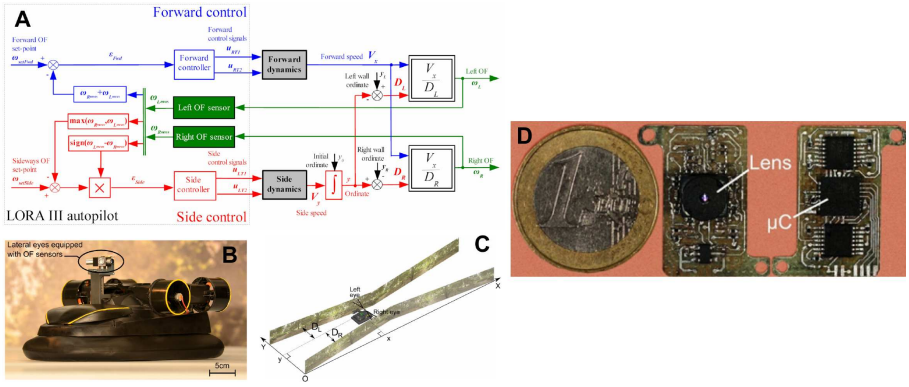

Fig. 12. A: LORA III autopilot enabling a hovercraft to navigate in a corridor by controlling its forward speed and its distance to the walls jointly, without measuring any speeds or distances. B: Fully-autonomous sighted hovercraft equipped with miniature elementary eyes and a bio-inspired *dual lateral optic flow regulator*. C: The tapered corridor consisted of a 400-cm long corridor with a relatively wide entrance (95cm) and with a 46-cm wide constriction located midway, the lateral walls of which were lined with photographs of natural colored scenes (trees and bushes) D: Top view of the 1-gram microcontroller-based visual motion sensor (size: 23.3x12.3 mm). Adapted from[118,157]

and the number of degrees of freedom in the horizontal plane are similar to those of an aerial robot (a helicopter, for instance). The micro-hovercraft's heading is maintained along the X-axis of the corridor (Fig. 12C) by a heading lock system that compensates for any yaw disturbances by controlling the two rear thrusters differentially. This system mimics the honeybee's heading lock system, which is based on a polarized light compass and gives the insect an impressively straight course, even in the presence of wind.[158]

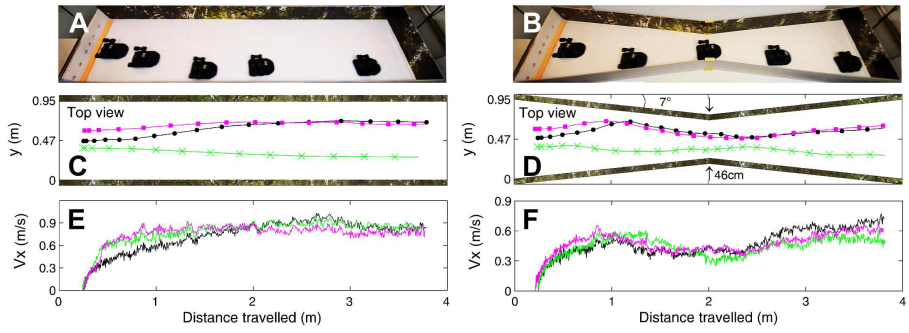

Fig. 13. A: LORA III autopilot enabling a hovercraft to navigate in a corridor by controlling its forward speed and its distance to the walls jointly, without measuring any speeds or distances. B: Fully-autonomous sighted hovercraft equipped with miniature elementary eyes and a bio-inspired *dual lateral optic flow regulator*, C: The tapered corridor consisted of a 400-cm long corridor with a relatively wide entrance (95cm) and with a 46-cm wide constriction located midway, the lateral walls of which were lined with photographs of natural colored scenes (trees and bushes). Adapted from

Figures 13 show real trajectories along a straight (Fig. 13A) and a tapered corridor (Fig. 13B) (tapering angle: 7°) with $\omega_{SetFwd} = 250°/s$ and $\omega_{SetSide} = 160°/s$ set-points. The LORA robot navigated safely and followed one of the two walls, regardless of its initial position y_0 at the entrance to the corridor. Whether in a straight (Fig. 13A) or tapered (Fig. 13B) corridor, the robot ended up by following either the right or the left wall in the steady state, depending on its initial ordinate y_0. These trajectories are typical of the wall-following behavior observed. The robot's speed profiles in the straight and tapered corridors (Figs. 13E and 13F) show that the LORA robot consistently adjusted its forward speed V_x to the local corridor width D. The LORA robot typically slowed down when the local corridor width decreased and speeded up when it widened out after the constriction.

In studying the types of operations that insects may perform to guide their flight on the basis of optic flow (OF) cues, we came up with several bio-inspired autopilot principles that harness the power of the translatory OF parsimoniously and therefore offer interesting prospects for MAV autonomous guidance. The micro-helicopter's outstanding visuomotor performance (Figs. 10) suggests how insects and MAVs may take off, follow terrain, and land if they are equipped with OF sensors facing the ground and an OF regulator that servos the measured OF to a given set-point (Fig. 9). The great advantage of this autopilot is that it requires neither to measure nor to compute nor to regulate (i.e., hold constant) any ground speeds or ground heights. The only variable it needs to measure and regulate is the OF — a variable that can be accessed straightforwardly by dedicated sensors called OF sensors.

6. Insect-based active vision for hyperacurate position sensing

In the previous sections 4 and 5, we have seen that motion detection depends on the measurement of a retinal slip speed (i.e., the optic flow) that is generated by locomotion. One of the main advantages of implementing active retinal micro-movements on artificial seeing systems is that they make it possible to detect and locate relevant stationary objects without any need of displacement and therefore without any need to move the whole body. In the angular position sensing device (PSD) described here, the micro-movements imposed on the photoreceptors were inspired by the retinal micro-scanning movements observed in the housefly's compound eye.[42]

6.1. *Principle of the hyperacurate sensor*

The hyperacurate sensor, Vibrating Optical Device for the Kontrol of Autonomous robots (VODKA),[65] was designed to estimate the azimuthal position of a vertically oriented contrasting target. Here we take the case of a sensor measuring the angular position of a vertical *edge* or bar.

The optical assembly comprising the two photoreceptors separates their optical axes by a constant angle denoted $\Delta\varphi$ (see Fig.17 and Fig.14), which is called the interreceptor angle. The sensor's main axis is defined as the bisector of these two

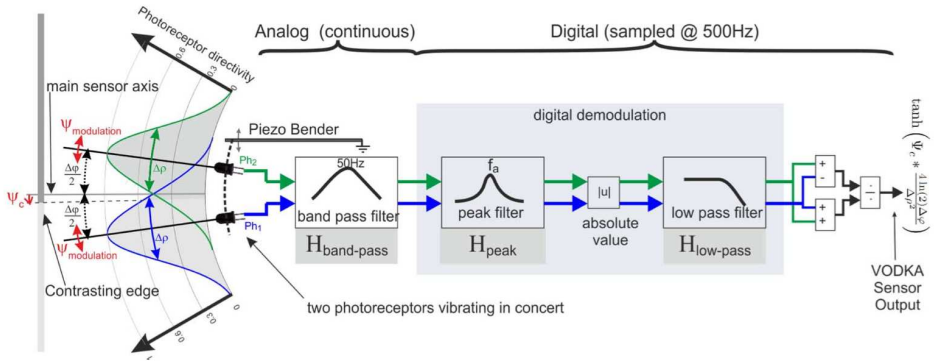

Fig. 14. Sketch diagram of the hyperacrate sensor. The left part shows the Gaussian angular sensitivity of each of the two photoreceptors placed in front of a contrasting edge. Mechanical vibration is applied to the two photoreceptors, causing their optical axes to rotate. A band-pass filter acting as a pseudo derivative extracts the signals generated by the relatively high frequency vibration (40Hz) of each photoreceptor axis. An optional peak filter removes all frequencies not associated with the vibration. A demodulator extracts the envelope of the signal. The relative difference between the two signals is computed as $(Ph'_1 - Ph'_2)/(Ph'_1 + Ph'_2)$ to yield the hyperacurate sensor output.. Adapted from[65]

axes. Each of the two photoreceptors' output signals, which are denoted $Ph_1$and Ph_2, depends on the angle between its optical axis and the target (the edge or the center of the bar). Let us take Ψ_c to denote the angular position of the visual target relative to the main hyperacurate sensor axes. The combined vibration of the two optical axes adds a high frequency modulation denoted Ψ_{mod}. The two photoreceptors' output signals can therefore be written as follows:

$$\begin{aligned} Ph_1(\Psi(t)) &= Ph\left(\Psi_c(t) + \Psi_{mod}(t) - \frac{\Delta\varphi}{2}\right) \\ Ph_2(\Psi(t)) &= Ph\left(\Psi_c(t) + \Psi_{mod}(t) + \frac{\Delta\varphi}{2}\right) \end{aligned} \tag{3}$$

where $\Psi(t) = \Psi_c(t) + \Psi_{mod}(t)$ and where:

- the following expression for Ph is used in the case of a contrasting edge;

$$\begin{aligned} Ph(\Psi_c) &= k\left(\frac{1}{2} + \int_{-\infty}^{\Psi_c} s(\Psi)\, d\Psi\right) \\ &= \frac{k}{2}\left(1 + erf\left(\frac{2\sqrt{\ln(2)} * \Psi_c}{\Delta\rho}\right)\right) \end{aligned} \tag{4}$$

where the factor k depends on both the contrast and the lighting conditions and erf is the so-called error function defined by:

$$erf(\Psi) = \frac{2}{\sqrt{\pi}} \int_0^{\Psi} e^{-x^2} dx \tag{5}$$

and the directivity function $s(\Psi)$ of a photoreceptor is therefore given by:

$$s(\Psi) = \frac{2\sqrt{\pi \ln(2)}}{\pi \Delta\rho} e^{-4 \ln(2) \frac{\Psi^2}{\Delta\rho^2}} \tag{6}$$

where Ψ is the angle between the photoreceptor optical axis and that of a point light source.

- the following expression for Ph in the case of a bar;

$$Ph(\Psi_c) = \frac{k}{2} \left(\text{erf} \left(\frac{2\sqrt{\ln(2)}(\Psi_c + \frac{L}{2})}{\Delta\rho} \right) - \text{erf} \left(\frac{2\sqrt{\ln(2)}(\Psi_c - \frac{L}{2})}{\Delta\rho} \right) \right) \tag{7}$$

To summarize, the hyperacurate sensor principle mainly involves the following:

- a Gaussian-like angular sensitivity function for each photoreceptor, mimicking the angular sensitivity function of flies' photoreceptors.[159]
- a joint micro-scanning movement of the two photoreceptors, mimicking the retinal micro-movements observed in single ommatidia of the fly compound eye.[101]
- a temporal derivative of the photoreceptor output signals, similar to the high pass filtering function occuring in the first order neuron of the fly's compound eye.

The hyperacurate sensor output signal results from the two photoreceptor signals, once they have been suitably processed in order to obtain *the ratio between the difference and the sum of the differentiated photodiode output signals.*

$$S_{VODKA} = \frac{\left| Ph_1'\big(\Psi(t)\big) \right| - \left| Ph_2'\big(\Psi(t)\big) \right|}{\left| Ph_1'\big(\Psi(t)\big) \right| + \left| Ph_2'\big(\Psi(t)\big) \right|} \tag{8}$$

where $\Psi(t)$ is the sum of the angular position of the contrasting feature Ψ_c with the small vibration Ψ_{mod}.

The derivative filter used here was a classical analog band-pass filter ($H_{band-pass}$ in Fig.14), in which the high-pass filter section acts as the differentiator and the low-pass filter section reduces the high frequency noise and prevents the subsequent analog-to-digital conversion from undergoing any aliasing effects.

When the sensor is placed in front of an edge , developing the expression 8 yields a remarkably simplified expres-sion, under the assumption that:

(1) the amplitude of Ψ_{mod} is very small (thus, $\Psi_{mod} \approx 0$ but $\Psi'_{mod} \neq 0$) and

(2) the temporal variations of Ψ_c are much slower than those of Ψ_{mod} (thus, $\Psi'_c \approx 0$ but $\Psi_c \neq 0$).

Under these conditions, the derivative of the two photoreceptors can be expressed as follows, using equation 6 and 4:

$$Ph'_1\big(\Psi(t)\big) = k * \frac{\sqrt{\pi \ln(2)}\Psi'(t)}{\pi\Delta\rho} * e^{-4\ln(2)\frac{(\Psi(t)-\frac{\Delta\varphi}{2})^2}{\Delta\rho^2}} \tag{9}$$

$$Ph'_2\big(\Psi(t)\big) = k * \frac{\sqrt{\pi \ln(2)}\Psi'(t)}{\pi\Delta\rho} * e^{-4\ln(2)\frac{(\Psi(t)+\frac{\Delta\varphi}{2})^2}{\Delta\rho^2}} \tag{10}$$

Substituting 8 into 10 gives, after some rewriting:

$$S_{VODKA} = \tanh\left(\Psi_c * \frac{4\ln(2)\Delta\varphi}{\Delta\rho^2}\right) \tag{11}$$

This remarkably simple expression gives the theoretical value of the hyperacurate sensor output as a function of the angular position Ψ_c of a contrasting edge present in its FOV. The characteristic curve plotted in Fig.15(a) is this *hyperbolic tangent function*, that is, an even, monotonic function of the angular position Ψ_c. The central part of the characteristic curve varies quasi linearly with the angular position Ψ_c, which makes the sensor capable of locating the angular position of a contrasting edge with great accuracy.

When the sensor is placed in front of a contrasting *bar*, developing the expression S_{VODKA} [8 with the temporal derivative of 7] does not simplify easily. However, the expression obtained is still an even function, as shown in Fig.15(b). It can be seen from this Figure that apart from the two "glitches" located at $\pm\Delta\varphi/2$, the characteristic curve obtained in the case of a *bar* is fairly similar to that obtained in the case of an *edge* (Fig.15(a) and (b)).

6.2. *Noteworthy features of the hyperacurate sensor*

We describe in this section several properties which make the hyperacurate visual sensor very usefull for locating contrasting objects in a natural environment.

6.2.1. *Robustness to lighting conditions*

The temporal derivation implemented in the band-pass filter (see Figure 14) amplifies high frequencies and removes the DC component from each photoreceptor output signal. Very large AC signal gain amplification can be obtained since the DC value is filtered out. These filtering and amplification steps in the signal processing make the hyperacurate sensor robust to the lighting conditions (affecting the DC value) at this early stage in the signal processing.

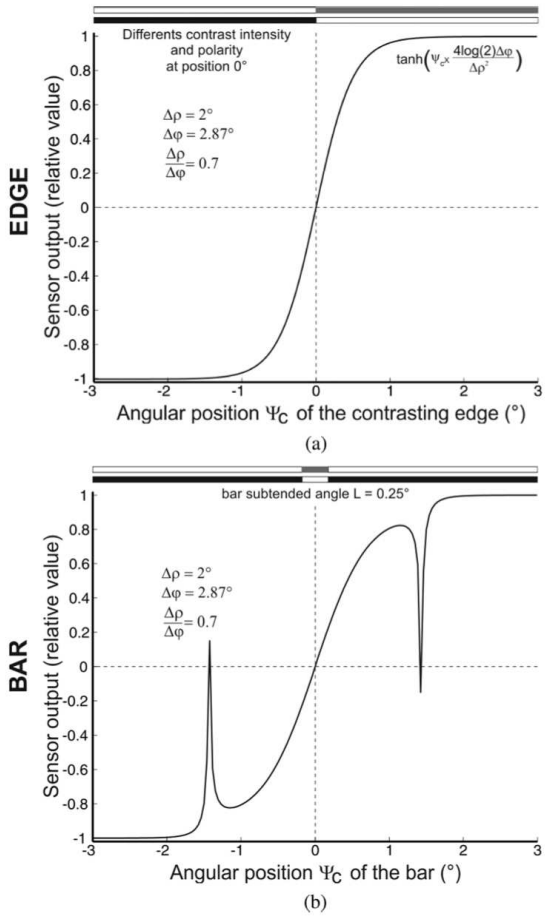

Fig. 15. Sketch diagram of the hyperacrate sensor. The left part shows the Gaussian angular sensitivity of each of the two photoreceptors placed in front of a contrasting edge. Mechanical vibration is applied to the two photoreceptors, causing their optical axes to rotate. A band-pass filter acting as a pseudo derivative extracts the signals generated by the relatively high frequency vibration (40Hz) of each photoreceptor axis. An optional peak filter removes all frequencies not associated with the vibration. A demodulator extracts the envelope of the signal. The relative difference between the two signals is computed as $(Ph'_1 - Ph'_2)/(Ph'_1 + Ph'_2)$ to yield the hyperacurate sensor output.. Adapted from[65]

6.2.2. *Robustness to contrast value and contrast polarity*

It is the absolute value of signals Ph'_1 and Ph'_2 that is used in Eq.8. The sensor is therefore insensitive to the polarity of the contrasting feature encountered (an *edge* or a *bar*), that is, it will respond equally to a white-to-dark or a dark-to-white target.

By calculating the relative difference (with expression Eq.8), the influence of contrast (modeled by the factor k in equations 4 and 7) can be removed. However,

this is a theoretical result, and the experimental data obtained with the sensor we implemented show a minimum detectable contrast m (Eq.12) of about 5%.

$$m = \frac{I_1 - I_2}{I_1 + I_2} \tag{12}$$

where the light intensities I_1 and I_2 are the higher and lower luminances measured on the two surfaces, respectivly (I_1 and I_2 measured with a similar photoreceptor to the VODKA photoreceptors).

6.2.3. *Robustness to vibration types*

Joint vibration of the two optical axes affects the signals delivered by both photoreceptors. From the amplitude of these signals, the angular position Ψ of a contrasting target lying in hyperacurate sensor visual field is obtained. From Eq.11, it can be seen that the vibration frequency has no influence on the ability of the sensor to detect the location of the target. Consequently, not only periodic signals such as sine waves but also random patterns of vibration can be used. For example, the "natural" undesirable vibration produced by the sensor's mechanical support (e.g., a robotic platform) can be exploited to drive the hyperacurate sensor's visual processing system.

According to the hyperacurate sensor principle described in section 6.1, a vibration pattern of some kind is a prerequisite to obtain hyperacuity, even though the type of vibration has no effect on the predicted sensor output. Taking the case of the low pass filter in the digital demodulation scheme (see Fig. 14), for example, the best results will be obtained with relatively high frequency and low amplitude vibrations (because the derivative of the high frequency in Eq.10 counteracts the low vibration amplitude).

7. Bio-inspired gaze control strategies for aerial robots[a]

In this section, we will describe our latest aerial robot, which has been called OSCAR II (see Fig. 16). OSCAR II differs from the original (OSCAR I) robot[60] in that its eye is no longer mechanically coupled to the body: this configuration makes it possible for the gaze to be actively locked onto the target, whatever disturbances may be applied to the robot's body.

In the angular position sensing device (PSD), the micro-movements imposed on the photoreceptors were inspired by the retinal micro-scanning movements observed in the housefly's compound eye.[42]

The sensor described here is the last in a series of fly-inspired visual scanning sensors (cf. Fig. 17), which began in 1996 with a micro-scanning retina[54] ca-

[a]Part of this paper reprinted from L. Kerhuel, S. Viollet and N. Franceschini, IROS Conference, ©2007 with permission from IEEE and from L. Kerhuel, S. Viollet and N. Franceschini, IEEE Trans.on robotics, Vol. 26, pp. 307-319 with permission from IEEE.

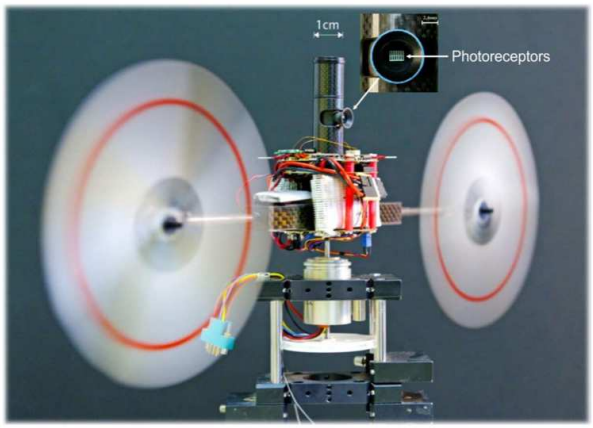

Fig. 16. OSCAR II robot equipped with the hyperacute sensor. The 100-gram aerial robot, which is usually suspended from the ceiling with a long $100\mu m$ nylon wire, controls its yaw on the basis of what it sees. Here it was mounted on the axis of a frictionless resolver so that its heading could be accurately monitored. The twin-engine robot orients itself by driving its two propellers differentially. The inset shows the robot's retina (after the lens has been removed), which can be subjected to repetitive micro-translations at a frequency of 40Hz by means of a piezo-bender (see Fig. 17). The hyperacurate retina is composed of an Ic-Haus LS2C package comprising 2 rows and 6 columns of photoreceptors. The hyperacurate sensor actually uses only the two central columns.. Picture from[65]

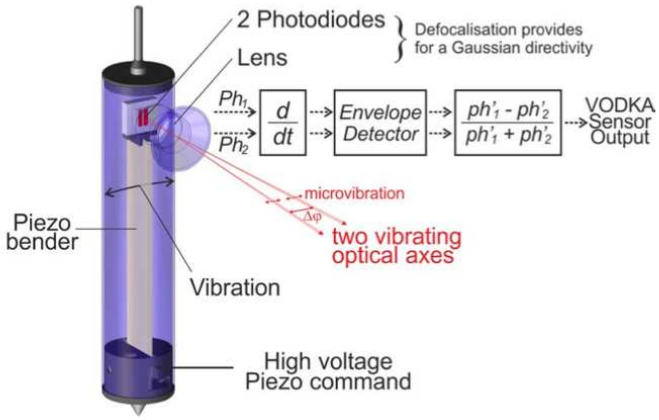

Fig. 17. CAD and sketch diagram of the hyperacurate sensor. The two photoreceptors are moved back and forth by a piezo-bender located inside the vertical eye tube, making their optical axes jointly scan a few degrees of the environment. The hyperacurate sensor's output is simply the relative difference between the two filtered photoreceptor signals Ph'_1 and Ph'_2. Adapted from[65]

pable of measuring low levels of translational optic flow, such as those perceived near the heading direction (the focus of expansion). This was followed by an-

other micro-scanning visual sensor[56] which enabled a small aerial robot to locate a moving target, fixate it and follow it smoothly ([57] and[60]). The ability to locate a contrasting feature (an edge or a bar) with greater spatial resolution than that imposed by the pixel pitch is known as hyperacuity.[160] Many visual sensors based on active retinal micro-movements have been used for various purposes: to enhance edge detection,[61,161,162] to improve obstacle avoidance,[54,55] or to read bar codes.[163] However, few studies have dealt so far with retinal vibrations in the context of hyperacuity. Visual scanning at a variable angular speed was previously used to enhance the resolution by a factor of 40 in an edge-locating task,[56] and more recently by a factor of 70. A pulsed-scanning mode was found to help a mobile robot detect the simple presence of edges in its visual field.[55] A circular micro- scanning mode was developed to improve the spatial resolution by transforming spatial information into temporal information.[67] This same mode was also used to obtain line or edge operators by correlating a modulating signal with the output signals emitted by a 2-D imager.[162] In humans, it has been established in theoretical studies that ocular micro-movements (tremor) can provide hyperacuity ([62,164,165]). Hyperacuity in artificial retinas has also been obtained without using any retinal micro-scanning processes, based on the overlapping Gaussian fields of view (FOV) of neighboring photoreceptors ([158,166–168]). However, unlike the sensors based on the present retinal micro-scanning approach, these static sensors cannot cope with different contrasting objects such as edges and bars, nor do they benefit from temporal signals to improve object detection.

In Section 7.1, we will describe the scheme underlying the fast accurate control of the "eye-in-head" angle and present the OSCAR II robot in section 7.2. In section 7.3, we will explain how we merged a gaze control system (GCS) with a heading control system (HCS). Finally, in section 7.4, we will discuss about a novel biomimetic "steering by gazing" control strategy.

7.1. *Eye-in-head or head-in-body movements : a key to forward visuomotor control*

Many studies have been published on how the gaze is held still in vertebrates and invertebrates, despite the disturbances to which the head (or body) is subjected. For example, in humans, the Rotational Vestibulo Ocular Reflex (RVOR,[169]) triggers a compensatory eye rotation of equal and opposite magnitude to the head rotation, so that the line of sight (the gaze) is stabilized. Studies on the human RVOR have shown that this inertial system responds efficiently with a latency of only about 10ms to sinusoidal head rotations with frequencies of up to 4 Hz[170] or even 6Hz,[171] as well as to step rotations.[172] Rhesus monkeys show very high VOR performances in the 0.5-5Hz[92] and even 5-25Hz[93] frequency ranges, which means that monkeys are able to reject both slow and fast disturbances throughout this wide range of frequencies. The fly itself possesses an exquisite VOR-like reflex controlling the orientation of its head.[173] Figure 18 illustrates the outstanding performances achieved by the gaze

stabilization systems of two different birds and a sandwasp. In the latter case, the authors nicely showed how the roll compensation reflex functioned in a wasp in free flight by maintaining the head fixed in space in spite of dramatic body rolls (amplitude up to 120° peak to peak) made to counter any lateral displacements.[174] Cancelling head roll prevents the wasp's visual system from being stimulated and therefore disturbed by rotational movements.[76]

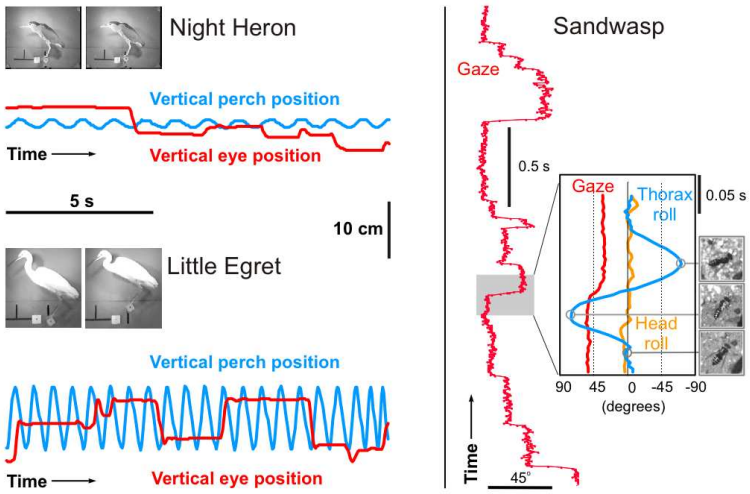

Fig. 18. Gaze stabilization in birds and insects. Left: A night heron, Nycticorax nycticorax (top) and a little egret, Egretta garzetta (bottom) standing on a vertically oscillating perch. Note the long periods of perfectly stable eye position, interrupted by brief re-positioning head movements (From[175]). Right: Horizontal gaze direction and head roll stabilization in a sandwasp (Bembix sp). Inset on the right shows thorax and head roll movements during a fast sideways translation to the left (see pictures) and a concurrent saccadic gaze shift to the right (From[174]). Figure and legend reproduced from Zeil et al. with permission from Elsevier.

In short, gaze stabilization seems to be a crucial ability for every animal capable of visually guided behavior. Even primitive animals such as the box jellyfish seem to be endowed with an exquisite mechanical stabilization system that holds the eyes oriented along the field of gravity.[176]

7.2. *Description of the OSCAR II robot*

OSCAR II is a miniature $(100 - gram)$ cordless twin-engine aerial robot equipped with a single-axis (yaw) oculomotor mechanism (Fig. 19).

The robot is able to adjust its heading accurately about the yaw axis by driving its two propellers differentially via a custom-made dual sensorless speed governor.[177] The robot's "body" consists of a carbon casing supporting the two motors. This casing is prolonged on each side by a hollow carbon beam within which the propeller drive shaft can rotate on miniature ball bearings. The robot's "head" is a large

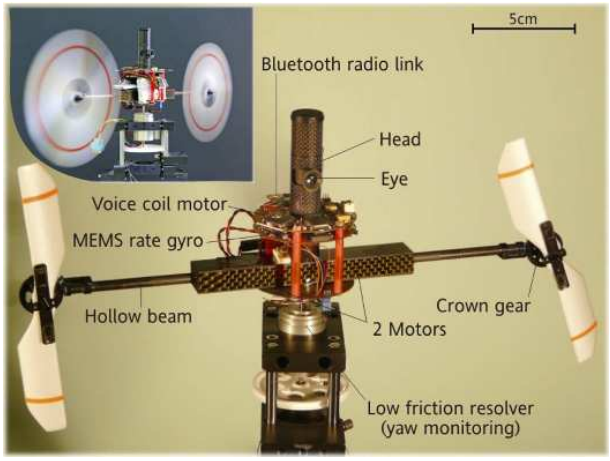

Fig. 19. OSCAR II is a 100-gram aerial robot that is able to control its heading about one axis (the vertical, yaw axis) by driving its two propellers differentially on the basis of what it sees. The eye of OSCAR II is mechanically uncoupled from the head, which is itself fixed to the "body". A gaze control system (GCS) enables the robot to fixate a target (a vertical white-dark edge placed 1 meter ahead) and to stabilize its gaze despite any severe disturbances (gusts of wind, slaps) that may affect its body. A heading control system (HCS), combined with the GCS, makes the robot's heading catch up with the gaze, which stabilizes the heading in the gaze direction. OSCAR II is mounted on a low-friction, low-inertia resolver, so that its heading can be monitored. Picture from[135]

(diameter 15mm) carbon tube mounted vertically on the motor casing. Within the head, an inner carbon "eye tube" mounted on pivot bearings can turn freely about the yaw axis.

The robot's eye consists of a miniature lens (diameter 5mm, focal length 8.5mm), behind which an elementary "retina" composed of a single pair of matched PIN photodiodes scans the surroundings at a frequency of 10Hz by means of a fast piezo actuator (Physik Instrumente) driven by an onboard waveform generator circuit (for details, see[63]). The retinal microscanning movement adopted here was inspired by our findings on the fly's compound eye.[42] The microscanning of the two photoreceptors occurs perpendicularly to the lens' axis, making their line-of-sights deviate periodically in concert. For details on the whys and wherefores of the particular microscanning law adopted, readers can consult our original analyses and simulations of the OSCAR sensor principle.[56] Basically, we showed that by associating an exponential scan with an Elementary Motion Detector (EMD), one can obtain a genuine Angular Position Sensor that is able to sense the position of an edge or a bar with great accuracy within the relatively small field-of-view available ($FOV = \pm 1.4°$, which is roughly equal to that of the human fovea). Interestingly, this sensor boasts a 40-fold better angular resolution than the inter-receptor angle in the task of locating an edge, and can therefore be said to be endowed with hyperacuity.[160] Further details about the performances (accuracy, calibration) of this microscanning visual

sensor are available in.[63]

7.3. *Implementation of the robot's oculomotor system*

In the human oculomotor system, the extra-ocular muscles (EOM) are often deemed to serve contradictory functions. On the one hand, they are required to keep the gaze accurately fixated onto a steady target,[178] and on the other hand, they are required to rotate the eye with a very small response time: a saccade of moderate amplitude is triggered within only about 100 ms.[179] Figure 20 shows a top view scheme of the novel miniature oculomotor system we have built and installed in OSCAR II (Fig.19).

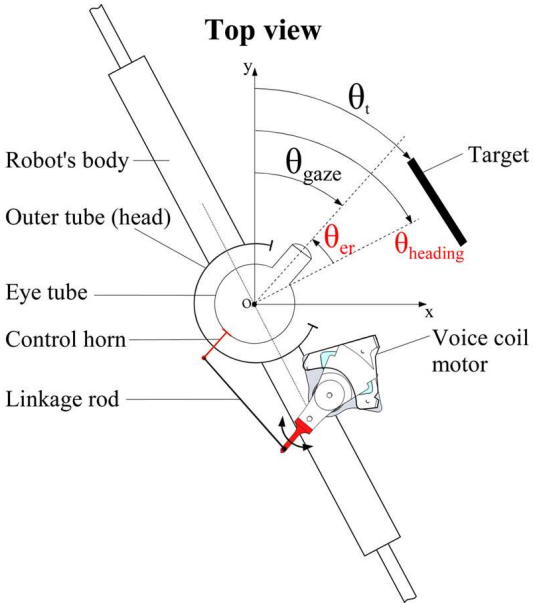

Fig. 20. The OSCAR II oculomotor mechanism (top view). The central eye tube (equipped with its two-pixel piezo-scanning retina, not shown here) is inserted into a larger carbon tube (the "head"), which is mounted onto the robot's body. The eye tube is mechanically uncoupled from the head with one degree of freedom about the yaw axis. The angle θ_{er} between the robot's heading and the direction of the gaze is finely controlled (via the linkage rod and the control horn) by a micro Voice Coil Motor (VCM) that was milled out from a hard disk microdrive. The visual sensor's output is a linear, even function of $\theta_t - \theta_{gaze}$; it delivers 0 Volts when the gaze is aligned with the target (i.e., $\theta_{gaze} = \theta_t$). Adapted from[180]

The high performance human oculomotor system was mimicked by controlling the orientation of the eye-tube with an unconventional extra-ocular actuator: a Voice Coil Motor (VCM), which was initially part of a hard disk microdrive (Hitachi). A VCM is normally used to displace the read-write head in disk drive control systems[181] and it works without making any trade-off between high positional ac-

curacy and fast displacement.

As VCM control requires an efficient position feedback loop. Whereas a simple PID controller was used in the original version,[180] we now used a state space approach by integrating a controller composed of an estimator cascaded with a state-augmented control gain K_{e0} (cf. figure 21) computed with a classical LQG method. This structure was used to servo the angular "eye in robot" position θ_{er} to the reference input U_{er} (see figure 20). θ_{er} was measured by placing a tiny Hall effect sensor in front of a micro magnet ($1mm^3$) glued to the eye-tube's rotation axis.

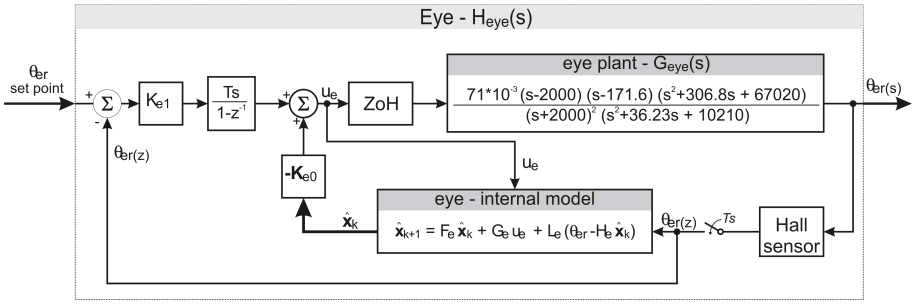

Fig. 21. Block diagram of the Voice Coil Motor (VCM) servo system, which servoes the "eye in robot" angle θ_{er} (see figure 20) to the reference $\theta_{er\ set\ point}$. In the internal state space model of the eye, both the command $U_e(z)$ and the measured angle $\theta_{er}(z)$ serve to estimate the 4 internal states of the eye's model, including its VCM actuator. The fifth external state is the integral of the eye's position error. A zero steady state error is classically obtained by augmenting the state vector and integrating the resulting angular position error. Figure from[135]

The step response shown in Figure 5 shows the very fast dynamics obtained with the closed-loop control of the eye-in-robot orientation, θ_{er}. We determined a rise time Trise as small as 19ms and a settling time Tsettle as small as 29ms (as compared to 44ms in the original version). With a 45-deg step (not shown here), a velocity peak of 2300°/s was reached, which is much higher than the 660°/s reached by our former PID controller[180] and much higher than the saturation velocity (800°/s) of the human eye measured during a saccade.[91] Unlike our robot's oculomotor control system (which is essentially linear), the human oculomotor control system is nonlinear, since the rise time increases typically with the saccade amplitude.[179]

7.4. *"Steering by gazing" control strategy*

The "steering by gazing" control strategy presented here amounts to maintaining the gaze automatically oriented toward a stationary (or moving) target and then ensuring that the robot's heading will catch up with the gaze direction, despite any disturbances encountered by the body. Two distinct but interdependent control schemes are at work in this system. The one is in charge of the robot's gaze, and the other is in charge of the robot's heading. The eye dynamics is very fast in

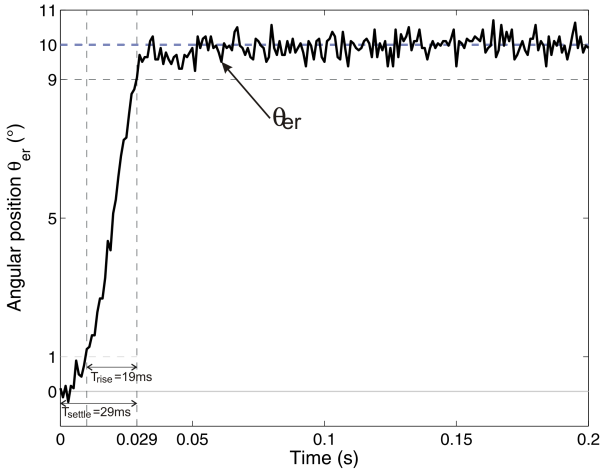

Fig. 22. Closed-loop step response of the "Eye in Robot" angular position θ_{er} to a large (10 degrees) step input applied to the reference input $\theta_{er\ set\ point}$ (cf. figure 21). The voice coil motor actuator is controlled via a full state feedback controller that makes the settling time (T_{settle}) as small as 29ms. The angular position θ_{er} is measured with a miniature Hall sensor placed in front of a tiny magnet glued onto the eye's axis. Figure from[135]

comparison with the robot's body dynamics. Our control strategy makes the robot minimize its retinal error signal and its heading error signal without requiring any knowledge of the robot's absolute angular position or that of the target. The fast phase of the heading dynamics depends on the inertial sensor (the rate gyro), while the slow phase (steady state) depends on the visual sensor. Here we will describe the eye control system and the heading control system and explain how they interact.

7.4.1. *Eye-Control strategy*

Figure 20 s hows a top view of the robot, where the various angles are defined.

Figure 23 summarizes the feedforward and feedback control systems involved in the eye control system. The feedback control system (depicted in the bottom of Fig. 23) is a regulator that keeps the retinal error $\epsilon_r = \theta_{target} - \theta_{gaze}$ at zero by adjusting the robot's eye orientation θ_{er}. The gaze-control strategy ensures that θ_{gaze} will follow any changes in the target position (θ_{target}). When the OSCAR II robot is presented with a stationary target, the eye control system will compensate for any disturbances applied to the body by holding the gaze, which is locked onto the target, due to the VOR and to the fast dynamics of the eye. If the target happens to move, the VFR will adjust the gaze orientation θ_{gaze} via θ_{er} so that the gaze will track the target smoothly, whatever the yaw disturbances possibly affecting the robot's body.

(1) Inertial Feedforward Control Loop (Vestibulo-ocular Re-flex): Like the semi-circular canals in the inner ear, which estimate the head's angular speeds,[182]

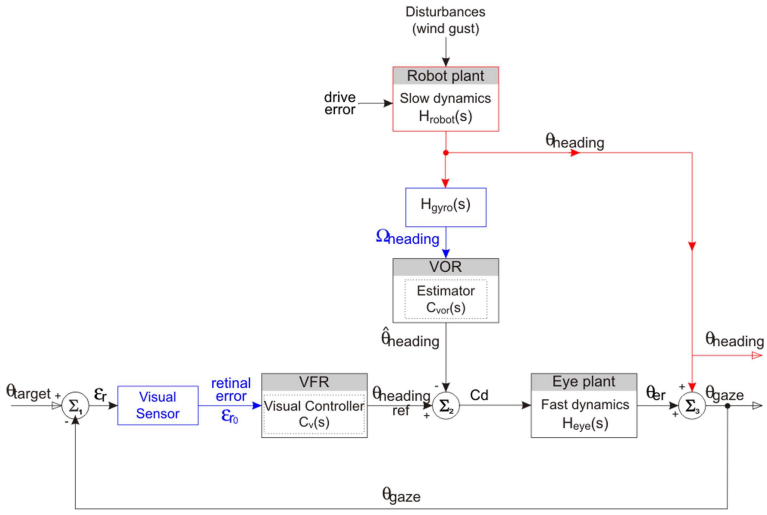

Fig. 23. ORs. The visual feedback loop at the bottom (which is called the VFR) is a position servo designed to minimize the retinal error measured $\epsilon_r = \theta_{target} - \theta_{gaze}$, thus making the eye lock onto a contrasting target. The feedforward controller (i.e., VOR) makes the eye compensate exactly for any dynamic changes in the robot's heading ($\theta_{heading}$). In Σ_3, the orientation of the robot $\theta_{heading}$ is added to the eye-in-robot orientation θ_{er}, and in Σ_2, the estimated heading $\hat{\theta}_{heading}$ is subtracted from the visual controller's output to hold the gaze steadily on the target, despite any heading disturbances. Note that the robot controls its gaze on the basis of measurements ($\Omega_{heading}$, ϵ_r) that relate entirely to its own coordinate frame: It requires no knowledge of the absolute heading ($\theta_{heading}$) or the absolute angular target position (θ_{target}), as shown in Fig. 20. Adapted from[135]

the microelectromechanical system (MEMS) rate gyro measures the robot's angular speed $\Omega_{heading}$ about the yaw axis. This measurement is integrated by a pseudointegrator ($C_{vor}(s)$) that estimates the body's orientation $\theta_{heading}$ in $\hat{\theta}_{heading}$ (see Fig. 23). The high-pass filter in $C_{vor}(s)$ has a low cutoff frequency of 0.05 Hz to overcome the slow and unpredictable drift, which is inherent to the MEMS rate gyro. The VOR was designed to compensate for any changes in $\theta_{heading}$ by faithfully making θ_{er} follow any change in $\hat{\theta}_{heading}$ with opposite sign (Σ_2).

(2) Visual Feedback Loop: The visual feedback loop strives to annul the retinal signal error ϵ_r to keep the robot's gaze locked onto the visual target. The embedded visual sensor measures the retinal error ϵ_r in the robot's reference frame (the robot, therefore, does not care whether the visual target is moving or not). The visual sensor's output ϵ_{r0} is a linear, even function of $\epsilon_r = \theta_{target} - \theta_{gaze}$. The visual feedback loop enables the robot to:

- fixate a stationary target;
- track a moving target;
- correct any low-frequency inaccuracies (i.e., drift) of the VOR inertial sensor.

The OSCAR II visual sensor[56] has a refresh rate of 10 Hz. This 10-Hz scanning of the visual scene is the main limiting factor involved in the process of visually rejecting any fast disturbances liable to destabilize the robot. Nonetheless, the VOR reflex solves this problem by greatly improving the dynamics of the gaze stabilization, thus preventing the target from straying beyond the narrow ($\pm 1.8°$) field of view (FOV) of the eye, even in the presence of strong aerodynamic disturbances.

7.4.2. *Heading Control Strategy*

The "steering-by-gazing" control strategy is an extension of the eye control strategy, as depicted in Fig. 21.

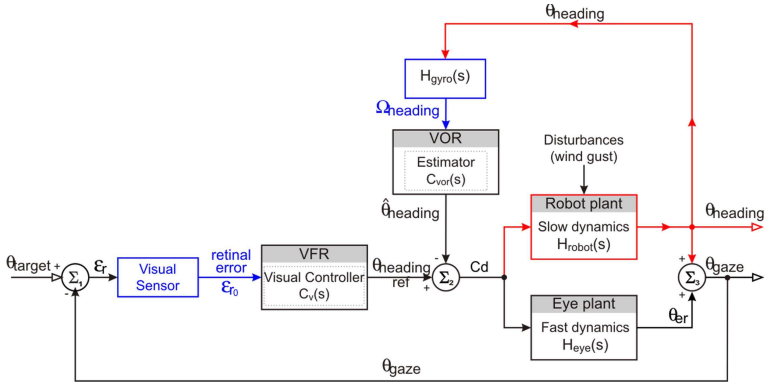

Fig. 24. Generic block diagram of the "the steering-by-gazing" control strategy that involves (bottom loop) two intertwined visual and (upper loop) inertial control system. The system cancels the retinal error signal ϵ_r by acting on both $\theta_{heading}$ and θ_{er}. The three signals θ_{er}, $\Omega_{heading}$, and retinal error ϵ_r (in blue) are measured in the robot's reference frame. None of the angle data available in the laboratory reference frame are conveyed to the controller. This system can be described in terms of Main–Vernier loops,[183] where the common drive signal (C_d) provides the (slow) heading feedback loop with an error signal and the (fast) eye dynamic loop with a set-point signal to control the gaze (θ_{gaze}). This novel control system meets the following two objectives: 1) keeping the gaze locked onto the visual (stationary or moving) target whatever aerodynamic disturbances (i.e., gusts of wind, ground effects, etc.) affect the robot's body and 2) automatically realigning the robot's heading $\theta_{heading}$ with the gaze and, hence, with the visual target. Adapted from[135]

In the generic control system, which is shown in Fig. 24, both the robot's steering dynamics and the eye dynamics are under the control of the common drive signal C_d; the gaze-control system and the heading control system are therefore interdependent. Any change in the robot's heading is treated like an input disturbance to the feedback gaze-control system. The common drive signal is the difference (see Σ_2 in Fig. 24) between the visual-fixation reflex (VFR) and the VOR signals. It drives both the eye (with its fast dynamics) and the robot (with its slow dynamics). The common drive signal (C_d) acts as a set-point for the eye orientation θ_{er} but as an error input signal for the robot's heading orientation $\theta_{heading}$ (see Fig. 25).

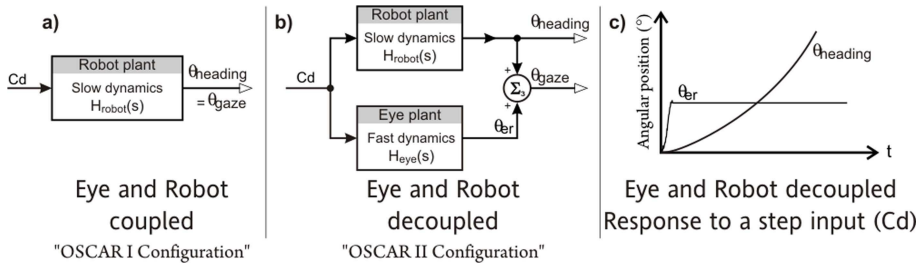

Fig. 25. (a) Classical (i.e., OSCAR I) robot configuration, where the eye is coupled to the body. (b) New (i.e., OSCAR II) robot configuration, where the eye is decoupled from the body. In our "Steering-by-gazing" control strategy, a common drive signal C_d controls both the eye and the robot. This common drive signal is an angular set-point for the eye (θ_{er}) and an angular error signal for the robot's heading ($\theta_{heading}$). (c) Step response of the eye θ_{er} and that of the robot's heading $\theta_{heading}$. When serving as an error signal controlling the robot's ($H_{robot}(s)$), C_d makes the robot rotate until C_d is cancelled; when serving as an angular set-point controlling the eye (θ_{er}), C_d makes the eye rotate until the appropriate position is reached. Adapted from[135]

This common drive signal causes the robot's body to rotate until its heading is aligned with its gaze (at which time $C_d = 0$). The visually guided behavior, which is implemented here, is therefore, such that the main output regulated at 0 is the retinal error ϵ_r between the gaze and the orientation of the target (see Fig. 20). The advantage is that the robot at no time looses sight of the target in the presence of strong disturbances affecting the body. The overall system of regulation can be said to first align θ_{gaze} with θ_t (i.e., $\epsilon_r = 0$), and then, to turn the robot's body to align $\theta_{heading}$ with θ_{gaze} (i.e., $C_d = 0$).

7.4.3. *Rejection of Aerodynamic Perturbations*

The previous version of the OSCAR robot (i.e., OSCAR I) was prone to be easily destabilized by gusts of wind because its eye was mechanically coupled to its body. OSCAR II is a great improvement over OSCAR I, since the direction of its gaze is decoupled from its heading. The performance of the OSCAR II robot was compared, depending on whether its ORs were activated or not (inactivating the ORs on OSCAR II makes it equivalent to the former OSCAR I configuration, where the eye was fixed to the body). In preliminary experiments,[180] we gave slaps to the robot with a custom-made slapping machine. In the current experiment, we used a more natural perturbation. The experimental setup used for this purpose is presented in Fig. 26.

This fan generated airflow at a speed of up to $5.2m/s$. The airflow perturbation regime was controlled via a pulsewidth-modulated (PWM) signal generated by an acquisition board. To calibrate the ducted fan, various PWM duty cycle values were applied for 10s, and the airspeed measured was averaged over this time. To compare the performance of the OSCAR II and OSCAR I configurations, both the robot's heading$\theta_{heading}$ and the "eye-in-robot" orientation θ_{er} were measured, and

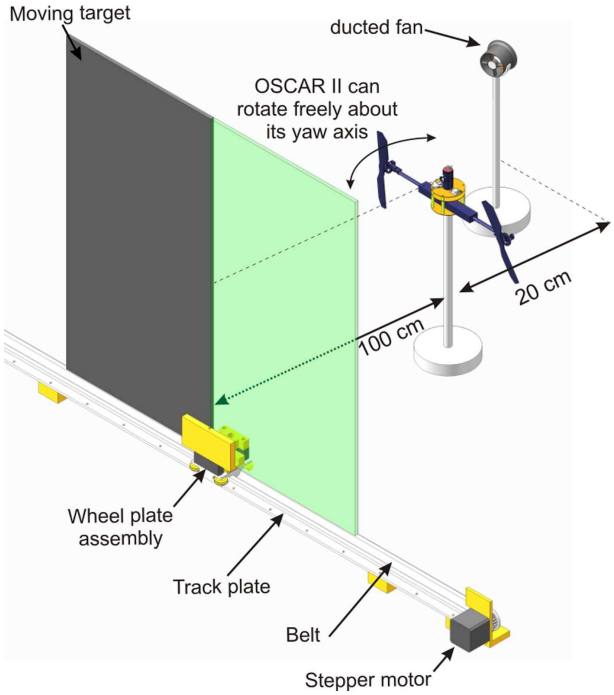

Fig. 26. Test bed used to assess the performance of the OSCAR II robot. The robot (see Fig. 19) is free to rotate frictionlessly about its yaw axis. It controls its heading by adjusting the rotational speeds of its two propellers differentially. OSCAR's gaze locks onto the target (an edge), which can be shifted in the frontal plane $1m$ ahead. During the tracking experiments, strong aerodynamic perturbations (gusts of wind at speeds of up to $6m/s$) were applied asymmetrically (i.e., onto one propeller) by means of a ducted fan placed $20cm$ behind one propeller. Adapted from[135]

the gaze θ_{gaze} was reconstructed as the sum (see Fig. 20).

$$\theta_{gaze} = \theta_{heading} - \theta_{er} \tag{13}$$

Figure 27 shows a close-up of the r obot's , eye's, and gaze's responses to the sudden gust of wind in the case of the OSCAR I configuration (see Fig. 27(a): ORs OFF) and the OSCAR II configuration (see Fig. 27(b): OR ON). In both experiments, the wind travel time between the fan and the robot is$240ms$. Despite the robot's inertial feedback controller (see Fig. 24), the sudden wind gust creates a peak heading error of 5°. After the 200-ms-long wind perturbation, the internal integrator compensates for the wind by making the contralateral propeller rotate faster. However, when the wind gust stops, the propeller differential speed of rotation makes the robot react in the opposite direction, thereby creating an error of opposite sign -3°.

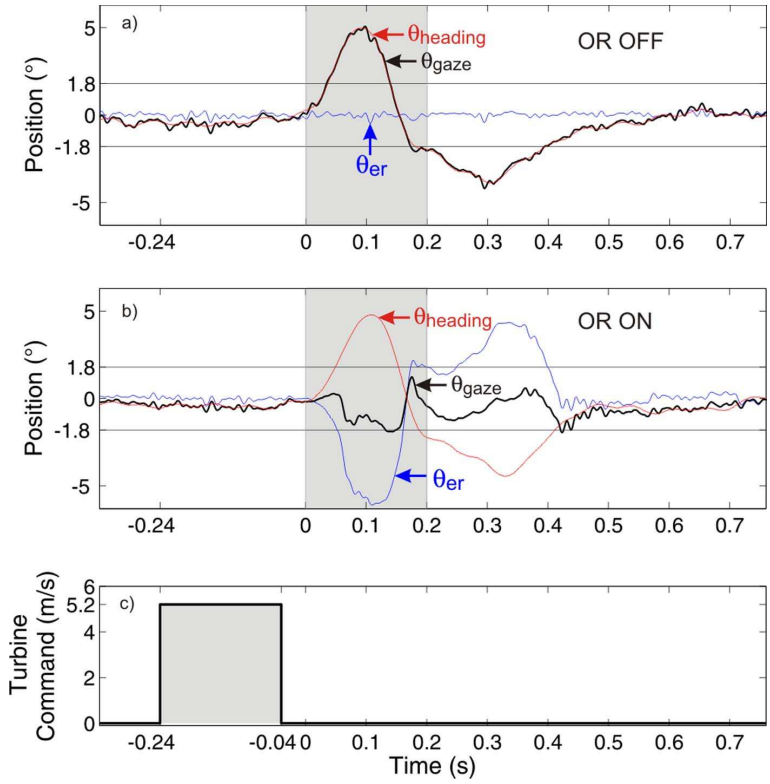

Fig. 27. (a) and (b) Visual fixation of a steady edge in the presence o f a 200-ms wind impulse by the OSCAR I configuration (without ORs) and the OSCAR II configuration (with ORs, i.e., VOR + VFR). In the OSCAR I configuration, the gaze can be seen to lead astray the ±1.8° limit (width of the FOV). Thus, the target, which is steady at the position 0 , gets out of the FOV and is lost for almost 400ms (0.03s until 0.4s). In the OSCAR II configuration, the "eye-in-robot" profile (θ_{er}, blue curve) shows that VOR immediately counteracts the robot rotation ($\theta_{heading}$, red curve) so that the gaze (θ_{gaze} , black curve) remains quasi-steady. This experiment demonstrates that in the OSCAR II configuration, the robot can maintain visual contact with the visual target, despite the strong aerial perturbation applied to its structure. Adapted from[135]

8. Conclusion

In studying the types of operations that insects may perform to guide their flight on the basis of optic flow cues, we came up with several bio-inspired autopilot principles that harness the power of the translatory optic flow parsimoniously and therefore offer interesting prospects for MAV autonomous guidance and navigation. Insect-inspired visuo-motor control systems can suggest robotic solutions requiring a much fewer pixels than the present-day mobile robots harnessed to computer-vision systems. First, we demonstrate on the tethered aerial robot called OCTAVE the optic flow regulation concept to perform complex tasks such as autonomous take off, autonomous terrain following, autonomous landing and autonomous compensation

for wind disturbances. LORA and Beerotor autopilots presented in section 5.4 were based on the *dual lateral optic flow regulation* principle. The autopilot causes the robot to automatically adjust its forward speed V_x to the local D-dimension of the corridor, while ensuring a safe clearance from the textured walls. This autopilot could also be applied to other types of vehicles such as blimps, autonomous underwater vehicles, and helicopters with counter-rotating rotors (in which pitch and roll are uncoupled).

Here we have also described how a miniature tethered aerial platform called OSCAR equipped with a one-axis, ultrafast accurate gaze control system inspired by highly proficient, long existing natural biological systems was designed and implemented. The seemingly complex gaze control system (Fig. 23) was designed to hold the robot's gaze fixated onto a contrasting object in spite of any major disturbances undergone by the body. It was established that after being destabilized by a nasty thump applied to its body, the robot:

- keeps fixating the target (despite the small visual field of its eye, which is no larger than that of the human fovea),
- reorients its heading actively until it is aligned with the gaze direction.

Reorientation is achieved rapidly, within about 0.6 seconds (Fig. 27). The important point here is that the gaze itself is the fundamental (Eulerian) reference parameter, on which all the relevant motor actions (orienting the "eye in robot" and the "robot in space") are based. This study considerably extends the scope of a former study, in which we developed a gaze control system but did not implement it onboard a robotic platform.[63] Besides, the oculomotor mechanism we are now using is a novel version based on a voice coil motor (VCM) taken from a hard disk microdrive. This actuator, which is able to orient the gaze with a settling time as short as $19ms$ (i.e., faster than a human ocular saccade), was the key to the development of our ultrafast gaze stabilization system.

Saccades, which have been studied in detail in humans, monkeys, and many insects, make it possible to orient the fovea onto a new target. This will be the subject of our further studies. We will now describe how saccadic movements can coexist with the oculomotor performance, which is described above. In the "steering-by-gazing" control strategy presented here, the robustness of the gaze-control system can be said to be extended to the heading control system. An aerial vehicle equipped with this system would be able to reject the aerodynamic disturbances encountered and to eventually realign its trajectory with the target on which the gaze remains firmly locked. This visuo-inertial heading control strategy is one step toward the development of autonomous unmanned air vehicles (UAVs) and autonomous underwater vehicles (AUVs). The lightness and low power consumption of the whole system would make it particularly suitable for application to MAVs and micro-underwater vehicles (MUVs), which are prone to disturbances due to untoward pitch variations, wing beats (or body undulations or fin beats), wind

gusts (or water streams), ground effects, vortices, and unpredictable aerodynamic (or hydrodynamic) disturbances of many other kinds. Lessons learned from biological creatures teach us that it is best to compensate early on for these disturbances, which was done here by using a visuo-inertial gaze-stabilization system as the basis for efficient heading stabilization. Anchoring the gaze on a contrasting feature in the environment provides a robust, drift-free starting point to explore the world.

Acknowledgment

The authors acknowledge the assistance of F. Paganucci and J. Diperi for constructing micro-mecanisms and M. Boyron for designing and producing the miniature electronic boards used here, including the piezo driver, the EMD, and the control systems. We thank J. Blanc for improving English. They also thank F. Colonnier, R. Juston, A. Manecy, and G. Sabiron for their work, the design and the realisation of their bio-inspred robot.

References

1. G. Card and M. H. Dickinson, Visually mediated motor planning in the escape response of drosophila, *Current Biology*. **In Press, Corrected Proof**, (2008). doi: 10.1016/j.cub.2008.07.094.
2. M. Giurfa and R. Menzel, Insect visual perception: complex abilities of simple nervous systems, *Current opinion in neurobiology*. **7**(4), 505–13 (Aug., 1997).
3. N. Strausfeld, *Atlas of an Insect Brain*. (Springer-Verlag, Berlin, Heidelberg, 1976).
4. K. Hausen, *Photoreception and vision in invertebrates*, chapter The lobula-complex of the fly: structure, function and signifiance in visual behaviour, pp. 523–559. Plenum, (1984).
5. M. Frye and M. Dickinson, Fly flight: A model for the neural control of complex behavior, *Neuron*. **32**(3), 385–388, (2001). ISSN 0896-6273. doi: 10.1016/S0896-6273(01)00490-1.
6. M. Heisenberg and R. Wolf, *Vision in Drosophila*. (Springer-Verlag, New York, 1984).
7. C. Blanes. Appareil visuel élementaire pour la navigation à vue d'un robot mobile autonome. Master's thesis, Master thesis in Neurosciences (DEA in French), Neurosciences, Univ. Aix-Marseille II, Advisor: N. Franceschini, (1986).
8. N. Franceschini, C. Blanes, and L. Oufar. Passive, noncontact optical velocity sensor. Technical Report No. 51549, ANVAR/DVAR, Paris, (1986).
9. J. Pichon, C. Blanes, and N. Franceschini, Visual guidance of a mobile robot equipped with a network of self-motion sensors, *Mobile robots*. **1195**, 44–53, (1989).
10. F. Ruffier and N. Franceschini. Octave, a bioinspired visuo-motor control system for the guidance of micro-air vehicles. In eds. A. Rodriguez-Vazquez, D. Abbott, and R. e. Carmona, *the proceedings of the Conference on Bioengineered and Bioinspired Systems, SPIE*, vol. 5119, pp. 1–12, Maspalomas, Spain (Mai, 2003). Belligham, USA.
11. F. Ruffier, S. Viollet, S. Amic, and N. Franceschini. Bio-inspired optical flow circuits for the visual guidance of micro-air vehicles. In *the proceedings of the IEEE International Symposium on Circuits and Systems (ISCAS)*, vol. 3, pp. 846–849, (2003).

12. G. Barrows. *Mixed-Mode VLSI Optic Flow Sensors for Micro Air Vehicles*. PhD thesis, University of Maryland, (1999).
13. G. Barrows and C. Neely. Mixed-mode VLSI optic flow sensors for in-flight control of a Micro Air Vehicle. In *in SPIE : Critical technologies for the future of computing*, vol. 4109, pp. 52–63, San Diego, CA, USA (Aug, 2000).
14. G. L. Barrows, C. Neely, and K. T. Miller. Optic flow sensors for mav navigation. In ed. AIAA, *Fixed and Flapping Wing Aerodynamics for Micro Air Vehicle Applications*, vol. 191, pp. 557–574, Bellingham, U.S.A. : Progress in Astronautics and Aeronautics, (2001).
15. W.-C. Wu, L. Schenato, R. Wood, and R. Fearing. Biomimetic sensor suite for flight control of a micromechanical flying insect: design and experimental results. In *Robotics and Automation, 2003. Proceedings. ICRA '03. IEEE International Conference on*, vol. 1, pp. 1146 – 1151 vol.1 (sept., 2003). doi: 10.1109/ROBOT.2003.1241747.
16. F. Ruffier and N. Franceschini. Visually guided micro-aerial vehicle: automatic take off, terrain following, landing and wind reaction. In *the proceedings of the IEEE International Conference on Robotics and Automation (ICRA 2004)*, (2004).
17. W. Green, P. Oh, and G. Barrows. Flying insect inspired vision for autonomous aerial robot maneuvers in near-earth environments. In *IEEE International Conference on Robotics and Automation (ICRA)*, (2004).
18. F. Ruffier and N. Franceschini, Optic flow regulation: the key to aircraft automatic guidance, *Robotics and Autonomous Systems*. **50**, 177–194, (2005).
19. R. Wood, S. Avadhanula, E. Steltz, M. Seeman, J. Entwistle, A. Bachrach, G. Barrows, and S. Sanders, An autonomous palm-sized gliding micro air vehicle, *Robotics Automation Magazine, IEEE*. **14**(2), 82 –91 (june, 2007). ISSN 1070-9932. doi: 10.1109/MRA.2007.380656.
20. A. Beyeler, J. Zufferey, and D. Floreano. optipilot: control of take-off and landing using optic flow. In *European Micro Aerial Vehicle Conference*, (2009).
21. A. Beyeler, J. C. Zufferey, and F. D., Vision-based control of near-obstacle flight, *Autonomous robots*. **27**, 201–219, (2009).
22. J.-C. Zufferey, A. Beyeler, and D. Floreano, Autonomous flight at low altitude using light sensors and little computational power, *International Journal of Micro Air Vehicles*. **2 (2)**, 107–117, (2010).
23. P.-E. Duhamel, N. Perez-Arancibia, G. Barrows, and R. Wood. Altitude feedback control of a flapping-wing microrobot using an on-board biologically inspired optical flow sensor. In *IEEE International Conference on Robotics and Automation (ICRA)*, Saint Paul, Minnesota, USA (May, 2012).
24. N. Franceschini, Early processing of colour and motion in a mosaic visual system, *Neurosc Res Suppl*. **2**, 517–549, (1985).
25. N. Franceschini, A. Riehle, and A. L. Nestour, *Facets of Vision*, chapter Directionally Selective Motion Detection by Insect Neurons, pp. 360–390. Springer-Verlag, (1989).
26. N. Franceschini, J. M. Pichon, and C. Blanes, From insect vision to robot vision, *Philosophical Transactions of the Royal Society B: Biological Sciences*. **337 (1281)**, 283–294, (1992).
27. J. S. Kennedy, Visual responses of flying mosquitoes, *Proceedings of the Zoogical Society of London*. **109**, 221–242, (1939).
28. J. Gibson, *The perception of the visual world*. (Houghton Mifflin, Boston, 1950).
29. J. S. Kennedy, The migration of the desert locust, *Philisophical Transactions of the Royal Society London*. **B 235**, 163–290, (1951).
30. D. N. Lee, The optic flow field: The foundation of vision, *Philisophical Transactions*

of the Royal Society London. **B 290**, 169–179, (1980).
31. J. Koenderink, Optic flow, *Biological Cybernetics*. **26**, 161–179, (1986).
32. F. Mura and N. Franceschini. Visual control of altitude and speed in a flying agent. In eds. J. A. Meyer and S. Wilson, *Conf on Simulation and Adaptive Behaviour*, pp. 91–100, (1994).
33. T. Netter and N. Franceschini, A robotic aircraft that follows terrain using a neuromorphic eye, *Intelligent Robots and Systems, 2008. IROS 2008. IEEE/RSJ International Conference on*. **1**, 129–134, (2002).
34. T. Neumann and H. Bülthoff, Behavior-oriented vision for biomimetic flight control, *Proceedings of the EPSRC/BBSRC International Workshop on Biologically Inspired Robotics: The Legacy of W. Grey Walter, 14-16 August 2002, HP Labs Bristol, UK*. **1**, 196–203, (2002).
35. F. Iida, Biologically inspired visual odometer for navigation of a flying robot, *Robotics and autonomous systems*. **44**, 201–208, (2003).
36. J. Chahl, M. Srinivasan, and S. Zhang, Landing strategies in honeybees and applications to uninhabited airborne vehicles, *The International Journal of Robotcs Research*. **23**, 101–110, (2004).
37. F. Ruffier. *PILOTE AUTOMATIQUE BIOMIMETIQUE Système générique inspiré du contrôle visuomoteur des insectes pour : le décollage, le suivi de terrain, la réaction au vent et látterrissage automatiques dún micro-aéronef*. PhD thesis, INP Grenoble, (2004).
38. X. Deng, L. Schenato, and S. Sastry, Flapping flight for biomimetic robotic insects: part ii-flight control design, *Robotics, IEEE Transactions on*. **22**(4), 789 –803 (aug., 2006). ISSN 1552-3098. doi: 10.1109/TRO.2006.875483.
39. J.-C. Zufferey, A. Beyeler, and D. Floreano. Insect-inspired Autonomous Microflyer. In *International Symposium on Flying Insects and Robots*, pp. 133–134, (2007).
40. S. Doncieux, *Evolution dárchitectures de contrôle pour robots volants*, chapter Intelligence Artificielle Située, pp. 109–127. Hermes, (1999).
41. J.-C. Zufferey, , D. Floreano, M. Van eeuwen, and T. Merenda. Evolving vison-based flying robots. In *In Bulthoff, Lee, Poggio, and Wallraven, editors, Proceedings of the 2nd International Workshop on Biologically Motivated Computer Vision LNCS*, (2002).
42. N. Franceschini and R. Chagneux. Repetitive scanning in the fly compound eye. In *Göttingen Neurobiology Report*, vol. 2. Thieme, (1997).
43. M. Garratt and J. Chahl, Vision-based terrain following for an unmanned rotorcraft, *Journal of Field Robotics*. **25**, 284–301, (2008).
44. B. Herisse, T. Hamel, R. Mahony, and F.-X. Russotto. A nonlinear terrain-following controller for a vtol unmanned aerial vehicle using translational optical flow. In *IEEE International Conference on Robotics and Automation*, pp. 3251–3257, Kobe, Japan, (2009).
45. B. Herisse, T. Hamel, R. Mahony, and F.-X. Russotto, Landing a vtol unmanned aerial vehicle on a moving platform using optical flow, *IEEE transaction on robotics*. **28**(1), 77–89, (2012).
46. J.-C. Zufferey and D. Floreano, Fly-inspired visual steering of ultralight indoor aircraft, *IEEE Transactions on Robotics*. **22(1)**, 137–146, (2006).
47. M. Land and T. Collett, *From Living Eyes to Seeing Machines*, chapter A Survey of Active Vision in Invertebrates, pp. 16–36. Oxford University Press, (1997).
48. S. Martinez-Conde, S. L. Macknik, and D. H. Hubel, The role of fixational eye movements in visual perception., *Nat Rev Neurosci*. **5**(3), 229–240 (Mar, 2004). doi: 10.1038/nrn1348.

49. D. C. Sandeman, Eye-scanning during walking in the crableptograpsus variegatus, *Journal of Comparative Physiology A: Neuroethology, Sensory, Neural, and Behavioral Physiology*. **124**, 249–257, (1978). ISSN 0340-7594. 10.1007/BF00657056.
50. R. L. Gregory, H. E. Ross, and N. Moray, The curious eye of copilia, *Nature*. **201** (4925), 1166–1168, (1964). doi: 10.1038/2011166a0.
51. B. Frost, Eye movements in daphnia pulex (de geer), *J Exp Biol*. **62**(1), 175–187, (1975).
52. M. F. Land, Movements of the retinae of jumping spiders (salticidae: dendryphantinae) in response to visual stimuli., *J Exp Biol*. **51**(2), 471–493 (Nov, 1969).
53. Kaps and Schmid, Mechanism and possible behavioural relevance of retinal movements in the ctenid spider cupiennius salei, *J Exp Biol*. **199**(Pt 11), 2451–2458, (1996).
54. F. Mura and N. Franceschini. Obstacle avoidance in a terrestrial mobile robot provided with a scanning retina. In *Proc. IEEE Intelligent Vehicles Symposium*, pp. 47–52 (19–20 Sept., 1996). doi: 10.1109/IVS.1996.566350.
55. F. Mura and I. Shimoyama. Visual guidance of a small mobile robot using active, biologically-inspired, eye movements. In *Proc. IEEE International Conference on Robotics and Automation*, vol. 3, pp. 1859–1864 (16–20 May, 1998). doi: 10.1109/ROBOT.1998.680513.
56. S. Viollet and N. Franceschini. Biologically-inspired visual scanning sensor for stabilization and tracking. In *Proceedings of the IEEE/RSJ International Conference on Intelligent Robots and Systems*, (1999).
57. S. Viollet and N. Franceschini. Visual servo system based on a biologically inspired scanning sensor. In *Sensor Fusion and Decentralized control in Robotics II*, vol. 3839, pp. 144–155. SPIE, (1999).
58. K. Hoshino, F. Mura, and I. Shimoyama, Design and performance of a micro-sized biomorphic compound eye with a scanning retina, *IEEE J. MEMS*. **9**(1), 32–37 (March, 2000). doi: 10.1109/84.825774.
59. K. Hoshino, F. Mura, and I. Shimoyama, A one-chip scanning retina with an integrated micromechanical scanning actuator, *IEEE J. MEMS*. **10**(4), 492–497 (Dec., 2001). doi: 10.1109/84.967370.
60. S. Viollet and N. Franceschini. Super-accurate visual control of an aerial minirobot. In eds. J. S. U. Rückert and U. W. (Eds), *Autonomous Minirobots for Research and Edutainment AMIRE*, number ISBN 3-935433-06-9, pp. 215–224. Heinz Nixdorf Institute, (2001).
61. M. O. Hongler, Y. L. de Meneses, A. Beyeler, and J. Jacot, The resonant retina: exploiting vibration noise to optimally detect edges in an image, *IEEE J. PAMI*. **25** (9), 1051–1062 (Sept., 2003). doi: 10.1109/TPAMI.2003.1227982.
62. M. H. Hennig and F. Wörgötter. Eye micro-movements improve stimulus detection beyond the nyquist limit in the peripheral retina. In *NIPS*, vol. 16. MIT press, (2004).
63. S. Viollet and N. Franceschini, A high speed gaze control system based on the vestibulo-ocular reflex, *Robotics and Autonomous systems*. **50**, 147–161, (2005).
64. S. Viollet and N. Franceschini, A hyperacute optical position sensor based on biomimetic retinal micro-scanning, *Sensors and Actuators A: Physical*. **160**(1-2), 60 – 68, (2010). ISSN 0924-4247. doi: DOI:10.1016/j.sna.2010.03.036.
65. L. Kerhuel, S. Viollet, and N. Franceschini, The vodka sensor: A bio-inspired hyperacute optical position sensing device, *IEEE Sensors Journal*. **12**(2), 315–324, (2012). doi: 10.1109/JSEN.2011.2129505.
66. R. Juston, S. Viollet, L. Kerhuel, and N. Franceschini, High performance optical angular position sensing at low-cost: a bio-inspired approach, *IEEE Sensors Journal*.

pp. 378–381, (2012). in revision.
67. O. Landolt and A. Mitros, Visual sensor with resolution enhancement by mechanical vibrations, *Autonomous Robots*. **11**(3), 233–239 (Nov., 2001).
68. T. S. Collett and M. F. Land, Visual control of flight behaviour in the hoverflysyritta pipiens l., *Journal of Comparative Physiology A: Neuroethology, Sensory, Neural, and Behavioral Physiology*. **99**(1), 1–66 (Mar., 1975).
69. R. Kern and D. Varju, Visual position stabilization in the hummingbird hawk moth, macroglossum stellatarum l., *J Comp Physiol A 182*. pp. 225–237, (1998).
70. N. Boeddeker, R. Kern, and M. Egelhaaf. Chasing a dummy target: smooth pursuit and velocity control in male blowflies. In *Proc. R. Soc. Lond.B 270*, pp. 393–399, (2003).
71. R. M. Olberg, R. C. Seaman, M. I. Coats, and A. F. Henry, Eye movements and target fixation during dragonfly prey-interception flights., *J Comp Physiol A Neuroethol Sens Neural Behav Physiol*. **193**(7), 685–693 (Jul, 2007). doi: 10.1007/s00359-007-0223-0.
72. C. Schilstra and J. H. van Hateren, Stabilizing gaze in flying blowflies., *Nature*. **395** (6703), 654 (Oct, 1998). doi: 10.1038/27114. URL `http://dx.doi.org/10.1038/27114`.
73. R. Hengstenberg, Mechanosensory control of compensatory head roll during flight in the blowfly calliphora erythrocephala meig, *J. Comp Physiol A*. **163**, 151–165, (1988).
74. D. C. Sandeman and H. Markl, Head movements in flies (calliphora) produced by deflexion of the halteres, *J Exp Biol*. **85**(1), 43–60 (Apr., 1980).
75. N. Boeddeker, L. Dittmar, W. Stürzl, and M. Egelhaaf, The fine structure of honeybee head and body yaw movements in a homing task., *Proc Biol Sci*. **277**(1689), 1899–1906 (Jun, 2010). doi: 10.1098/rspb.2009.2326.
76. S. Viollet and J. Zeil, Feed-forward and visual feed-back control of head roll orientation in wasps (polistes humilis, vespidae, hymenoptera), *Journal of Experimental Biology*. (2013). doi: doi:10.1242/jeb.074773.
77. T. Yamaguchi and H. Yamasaki. Velocity based vestibular-visual integration in active sensing system. In *Proc. IEEE Intern. Conf. on Multisensor Fusion and Integration for Intelligent System*, pp. 639–646, Las Vegas, USA, (1994).
78. T. Shibata, H. Tabata, S. Schaal, and M. Kawato, Biomimetic gaze stabilization based on feedback-error-learning with nonparametric regression networks, *Neural Networks*. **14**, 201–216, (2001).
79. F. Panerai, G. Metta, and G. Sandini, Learning visual stabilization reflexes in robots with moving eyes, *Neurocomputing*. **48**, 323–337, (2002).
80. A. Lewis. Visual navigation in a robot using zig-zag behavior. In *Proceedings of Neural Informations Processing Systems (NIPS)*, pp. 822–828, (1997).
81. P. Viola. Neurally inspired plasticity in oculomotor processes. In *Proceedings of Neural Informations Processing Systems (NIPS)*, pp. 290–297, (1989).
82. J.-A. Meyer, B. Guillot, A. andGirard, M. Khamassi, P. Pirim, and A. Berthoz, The psikharpax project: towards building an artificial rat, *Robotics and Autonomous Systems*. **50**(4), 211–223 (Mar., 2005).
83. R. Miyauchi, N. Shiroma, and F. Matsuno, Compact image stabilization system using camera posture information, *J of field robotics*. **25**, 268–283, (2008).
84. X. Twombly, R. Boyle, and S. Colombano. Active stabilization of images acquired on a walking robotic platform. In *Advances in visual computing. Part I-II : Second international symposium, ISVC 2006*, pp. 851–860, (2006).
85. F. Panerai, G. Metta, and G. Sandini. Learning vor-like stabilization reflexes in

robots. In *ESANN'2000 Proceedings*, pp. 95–102, Bruges,Belgium (April, 2000).
86. S. Takizawa, S. Ushida, T. Okatani, and K. Deguchi. 2dof motion stabilization of biped robot by gaze control strategy. In *Intelligent Robots and Systems, 2005. (IROS 2005). 2005 IEEE/RSJ International Conference on*, pp. 1102–1107 (2-6 Aug., 2005). doi: 10.1109/IROS.2005.1545562.
87. S. Ushida, K. Yoshimi, T. Okatani, and K. Deguchi. The importance of gaze control mechanism on vision-based motion control of a biped robot. In *Intelligent Robots and Systems, 2006 IEEE/RSJ International Conference on*, pp. 4447–4452 (Oct., 2006). doi: 10.1109/IROS.2006.282079.
88. M. N. Sreenivasa, P. Soueres, J.-P. Laumond, and A. Berthoz. Steering a humanoid robot by its head. In *Proc. IEEE/RSJ Int. Conf. Intelligent Robots and Systems IROS 2009*, pp. 4451–4456, (2009). doi: 10.1109/IROS.2009.5354503.
89. R. Wagner, I. W. Hunter, and H. L. Galiana. A fast robotic eye/head system: Eye design and performance. In *Proc. of IEEE Engineering in Medicine and Biology Society*, vol. 14, pp. 1584–1585, (1992).
90. A. Lenz, T. Balakrishnan, A. G. Pipe, and C. Melhuish, An adaptive gaze stabilization controller inspired by the vestibulo-ocular reflex., *Bioinspir Biomim.* **3**(3), 35001 (Sep, 2008). doi: 10.1088/1748-3182/3/3/035001.
91. E. Maini, L. Manfredi, C. Laschi, and P. Dario, Bioinspired velocity control of fast gaze shifts on a robotic anthropomorphic head, *Autonomous Robots.* **25**(1), 37–58 (Aug., 2008).
92. E. L. Keller, Gain of the vestibulo-ocular reflex in monkey at high rotational frequencies, *Vis. Res.* **18**, 311–115, (1978).
93. M. Huterer and K. E. Cullen, Vestibuloocular reflex dynamics during high-frequency and high acceleration rotations of the head on body in rhesus monkey, *J Neurophysiol.* **88**, 13–28, (2002).
94. R. W. Clifford, P. C. Know, and G. N. Dutton, Does extraocular muscle proprioception influence oculomotor control ?, *Br. J. Ophtalmol.* **84**, 1071–1074, (2000).
95. N. Dancause, M. Taylor, E. Plautz, J. Radel, T. Whittaker, R. Nudo, and A. Feldman, A stretch reflex in extraocular muscles of species purportedly lacking muscle spindles, *Exp Brain Res.* **180**(1), 15–21 (Jun, 2007). doi: 10.1007/s00221-006-0833-8.
96. T. Preuss and R. Hengstenberg, Structure and kinematics of the prosternal organs and their influence on head position in the blowfly calliphora erythrocephala meig, *J Comp Physiol A 171.* pp. 483–493, (1992).
97. E. Liske, The influence of head position on the flight behaviour of the fly, calliphora erythrocephala, *J. Insect Physiol.* **23**, 375–179, (1977).
98. N. Franceschini, Visual guidance based on optic flow: a biorobotic approach, *Journal of Physiology-Paris.* **98**(1-3), 281 – 292, (2004). ISSN 0928-4257. doi: 10.1016/j.jphysparis.2004.06.002.
99. C. Blanes. *Guidage visuel d'un robot mobile autonome d'inspiration bionique.* PhD thesis, INP Grenoble, (1991).
100. N. Franceschini, J. M. Pichon, and C. Blanes. Real time visuomotor control: from flies to robots. In *the proceedings of the IEEE Conference on Advanced Robotics (ICAR91)*, pp. 931–935, Pisa, Italy, (1991).
101. N. Franceschini, J. M. Pichon, and C. Blanes. Bionics of visuo-motor control. In ed. T. Gomi, *Evolutionary Robotics: From Intelligent Robots to Artificial Life*, pp. 49–67. AAI Books, Ottawa, (1997).
102. N. Franceschini, F. Ruffier, and J. Serres, Obstacle avoidance and speed control in insects and micro-aerial vehicles, *Acta Futura.* **3**(4), 15–34, (2009).
103. H. Wagner, Flight performance and visual control of flight of the free-flying housefly

(musca domestica l.) i. organization of the flight motor., *Philosophical Transactions of the Royal Society of London. Series B, Biological Sciences.* **312**, 527–551, (1986).
104. Schilstra and Hateren, Blowfly flight and optic flow. i. thorax kinematics and flight dynamics, *J Exp Biol.* **202 (Pt 11)**, 1481–1490 (Jun, 1999).
105. L. F. Tammero and M. H. Dickinson, The influence of visual landscape on the free flight behavior of the fruit fly drosophila melanogaster, *Journal of Experimental Biology.* **205**, 327–343, (2002).
106. N. Franceschini, F. Ruffier, and J. Serres, A bio-inspired flying robot sheds light on insect piloting abilities, *Current Biology.* **17**(4), 329–335, (2007).
107. F. Expert, S. Viollet, and F. Ruffier, Outdoor field performances of insect-based visual motion sensors, *Journal of Field Robotics.* **28 (4)**, 529–541, (2011).
108. J. Kramer, R. Sarpeshkar, and C. Koch, An analog VLSI velocity sensor, *in Proceedings of the* IEEE *International Symposium on Circuit and Systems (ISCAS).* **Seattle, WA, USA**, 413–416 (May, 1995).
109. R. Sarpeshkar, J. Kramer, G. Indiveri, and C. Koch, Analog vlsi architectures for motion processing: From fundamental limits to system applications, *Proceedings of the IEEE.* **84 (7)**, 969–987, (1996).
110. R. Moeckel and S. Liu, Motion detection circuits for a time-to-travel algorithm, *IEEE International Symposium on Circuits and Systems. (ISCAS).* **New orleans, LA, USA**, 3079–3082 (May, 2007).
111. S. Hrabar, G. Sukhatme, P. Corke, K. Usher, and J. Roberts. Combined optic-flow and stereo-based navigation of urban canyons for a uav. In *the proceedings of the International Conference on Intelligent Robots and Systems (IROS)*, pp. 3309–3316 (aug., 2005).
112. S. Griffiths, J. Saunders, A. Curtis, B. Barber, T. McLain, and R. Beard, Maximizing miniature aerial vehicles, *Robotics & Automation Magazine, IEEE.* **13**, 34–43, (2006).
113. J. Conroy, G. Gremillion, B. Ranganathan, and J. Humbert, Implementation of wide-field integration of optic flow for autonomous quadrotor navigation, *Autonomous Robots.* **27**, 189–198, (2009). ISSN 0929-5593.
114. F. Kendoul, K. Nonami, I. Fantoni, and R. Lozano, An adaptive vision-based autopilot for mini flying machines guidance, navigation and control, *Autonomous Robots.* **27**, 165–188, (2009).
115. Y. Watanabe, P. Fabiani, and G. Le Besnerais. Simultaneous visual target tracking and navigation in a gps-denied environment. In *the proceedings of the International Conference on Advanced Robotics (ICAR)*, pp. 1 –6 (june, 2009).
116. F. Roubieu, F. Expert, M. Boyron, B. Fuschlock, S. Viollet, and F. Ruffier. A novel 1-gram insect based device measuring visual motion along 5 optical directions. In *the proceedings of the IEEE Sensors conference*, pp. 687–690, Limerick, Ireland, (2011).
117. F. Expert, F. L. Roubieu, and F. Ruffier. Interpolation based "time of travel" scheme in a visual motion sensor using a small 2d retina. In *the proceedings of the IEEE Sensors Conference*, pp. 2231–2234, Taipei, Taiwan (October, 2012).
118. F. L. Roubieu, J. Serres, N. Franceschini, F. Ruffier, and S. Viollet. A fully-autonomous hovercraft inspired by bees; wall-following and speed control in straight and tapered corridors. In *IEEE International Conference on Robotics and Biomimetics (ROBIO)*, Guangzhou, China (December, 2012).
119. F. Ruffier and F. Expert. Visual motion sensing onboard a 50-g helicopter flying freely under complex VICON-lighting conditions. In *the proceedings of the International Conference on Complex Medical Engineering*, pp. 634–639, Kobe, Japan (July, 2012).
120. B. Hassenstein and W. Reichardt, Systemtheoretische Analyse der Zeit-, Reihenfolgen-, und Vorzeichenauswertung bei der Bewegungsperzeption des

Rüsselkafers, *Chlorophanus. Zeitschrift für Naturforschung.* **11**, 513–524, (1956).
121. R. R. Harrison and C. Koch, A robust analog VLSI motion sensor based on the visual system of the fly, *Autonomous robots.* **7**(3), 211–224, (1999).
122. S. Liu and A. Usseglio-Viretta, Fly-like visuomotor responses of a robot using aVLSI motion-sensitive chips, *Biological Cybernetics.* **85**, 449–457, (2001).
123. M. Srinivasan, An image-interpolation technique for the computation of optic flow and egomotion, *Biological Cybernetics.* **71**, 401–415, (1994).
124. J. Santos-Victor, G. Sandini, F. Curotto, and S. Garibaldi, Divergent stereo in autonomous navigation: From bees to robots, *International Journal of Computer Vision.* **14**, 159–177, (1995).
125. J. Barron, D. Fleet, and S. Beauchemin, Performance of optic flow techniques, *International Journal of Computer Vision.* **12**, 43–77, (1994).
126. R. Chan, A. Mulla, and K. Stol, Characterisation of low-cost optical flow sensors, *in Proceeding of the Australasian Conference on Robotics and Automation.* **Brisbane, Australia**, 1–8, (2010).
127. F. Expert, S. Viollet, and F. Ruffier. A mouse sensor and a 2-pixel motion sensor exposed to continuous illuminance changes. In *IEEE Sensors 2011 conference*, (2011).
128. J. D. Jackson, D. W. Callahan, and J. Marstrander, A rationale for the use of optical mice chips for economic and accurate vehicle tracking, *Proc. IEEE International Conference on Automation Science and Engineering CASE 2007.* **Scottsdale, AZ, USA**, 939–944, (Sept, 2007).
129. H. Dahmen, A. Millers, and H. A. Mallot, *Flying insects and robots*, chapter 9 : Insect inspired odometry by optic flow recorded with optical mouse chips, pp. 115–126. Springer, Berlin, Eds : Floreano, D. and Zufferey,J. C. and Srinivasan, M. V. and Ellington, C., (2009).
130. C. Bartolozzi and G. Indiveri, A selective attention multi-chip system with dynamic synapses and and integrate-and-fire neurons, *Advances in Neural Information Processing Systems.* **19**, 113–120, (2007).
131. R. S. A. Brinkworth and D. C. O'Carroll, Robust models for optic flow coding in natural scenes inspired by insect biology, *PLOS Computational Biology.* **5**, e1000555, (2009).
132. P. Xu, J. Humbert, and P. Abshire, Analog vlsi implementation of wide-field integration method, *Journal of Intelligent & Robotic Systems.* **Online**, 1–23, (2011). doi: 10.1007/s10846-011-9549-5.
133. C. Higgins and S. Shams, A biologically inspired modular VLSI system for visual measurement of self-motion, *IEEE Sensors.* **2**, 508–528, (2002).
134. R. Laviana, L. Carranza, S. Vargas, G. Linan, and E. Roca, A bioinspired vision chip architecture for collision detection in automotive applications, *in Proceedings of SPIE : Bioengineered and bioinspired systems II,Sevilla, Espana.* **5839**, 13–24, (May, 2005).
135. L. Kerhuel, S. Viollet, and N. Franceschini, Steering by gazing : an efficient biomimetic control strategy for visually guided micro aerial vehicles, *IEEE Transactions on robotics.* **26**, 307–319, (2010).
136. J. Díaz, E. Ros, R. Agis, and J. Bernier, Superpipelined high-performance optical-flow computation architecture, *Computer Vision and Image Understanding.* **112**, 262–273, (2008).
137. S. Viollet, F. Ruffier, T. Ray, M. Menouni, F. Aubépart, L. Kerhuel, and N. Franceschini. Characteristics of three miniature bio-inspired optic flow sensors in natural environments. In *In Proc. of the IEEE Conf. on Sensors Technologies and Applications, Sensorcomm*, pp. 51–55, (2010).

138. F. Expert and F. Ruffier. Controlling docking, altitude and speed in a circular high-roofed tunnel thanks to the optic flow. In *Intelligent Robots and Systems (IROS), 2012 IEEE/RSJ International Conference on*, pp. 1125–1132. IEEE, (2012).
139. G. Sabiron, P. Chavent, T. Raharijaona, P. Fabiani, and F. Ruffier. Low-speed optic-flow sensor onboard an unmanned helicopter flying outside over fields. In *the proceedings of the IEEE International Conference on Robotics and Automation (ICRA 2013)*, pp. 2253–2260, (2013).
140. N. Franceschini, Towards automatic visual guidance of aerospace vehicles : from insects to robots, *Acta Futura*. **3**, 15–34, (2009).
141. N. Franceschini, A. Riehl, and A. le Nestour, *Directionally Selective Motion Detection By Insect Neurons*. (In-Tech, 1989).
142. S. Ullman, Analysis of visual motion by biological and computer systems, *Computer*. **14**, 57–69, (1981). doi: 10.1109/C-M.1981.220564.
143. R. Benson and T. Delbrück, *Direction selective silicon retina that uses null inhibition*. (Morgan Kaufman, San Mateo, CA, 1992).
144. J. Koenderink and A. Doorn, Facts on optic flow, *Biological Cybernetics*. **56**, 247–254, (1987).
145. T. Delbrück and C. Mead. Adaptive photoreceptor with wide dynamic range. In *Circuits and Systems, 1994. ISCAS '94., 1994 IEEE International Symposium on*, vol. 4, pp. 339 –342 vol.4 (may-2 jun, 1994). doi: 10.1109/ISCAS.1994.409266.
146. F. Aubépart, M. Ménouni, T. Loubignac, B. Dinkelspieler, and N. Franceschini. Capteur de flux optique basé sur une rétine intégrée et un FPGA. In *Colloque Interdisciplinaire en Instrumentation*, pp. 508–520. Hermes, (2007).
147. T. Whiteside and G. Samuel, Blur zone, *Nature*. **225**, 94–95, (1970).
148. M. Ibboston, Evidence for velocity-tuned motion-sensitive descending neu-rons in the honeybee, *Proceedings of the Royal Society B: Biological Sciences*. **B 268**, 2195–201, (2001). doi: 10.1098/rspb.2009.1928.
149. M. V. Srinivasan, M. Lehrer, W. H. Kirchner, and S. Zhang, Range perception through apparent image speed in freely flying honeybees, *Visual Neuroscince*. **6**, 519–535, (1991).
150. E. Baird, M. V. Srinivasan, S. Zhang, and A. Cowling, Visual control of flight speed in honeybees, *J. Exp. Biol.* **208**, 3895–3905, (2005).
151. M. V. Srinivasan, S. W. Zhang, M. Lehrer, and T. S. Collett, Honeybee navigation en route to the goal: visual flight control and odometry, *Journal of Exprerimental Biology*. **199**, 237–244, (1996).
152. M. Srinivasan, S. Zhang, J. Chahl, E. Barth, and V. S., How honeybees make grazing landings on flat surfaces, *Biological Cybernetics*. **83**, 171–183, (2000).
153. E. Baird, M. V. Srinivasan, S. Zhang, R. Lamont, and A. Cowling, Visual control of flight speed and height in honeybee, *LNCS*. **4095**, 40–51, (2006).
154. A. D. Straw, S. Lee, and M. H. Dickinson, Visual control of altitude in flying drosophila, *Current Biology*. **20**(17), 1550–1556, (2010). ISSN 09609822.
155. M. Srinivasan, S. Thurrowgood, and D. Soccol. An optical system for guidance of terrain following in uavs. In *IEEE International Conference on Video and Signal Based Surveillance (AVSS)*, (2006).
156. J. Serres, G. Masson, F. Ruffier, and N. Franceschini, A bee in the corridor: centering and wall-following, *Naturwissenschaften*. **95**, 1181–1187, (2008).
157. J. Serres, D. Dray, F. Ruffier, and N. Franceschini, A vision-based autopilot for a miniature air vehicle: joint speed control and lateral obstacle avoidance, *Autonomous robot*. **25**, 103–122, (2008). doi: 10.1007/s10514-007-9069-0.
158. D. T. Riley, W. M. Harmann, S. F. Barrett, and C. H. G. Wright, Musca domestica

inspired machine vision sensor with hyperacuity, *Bioinspiration & Biomimetics*. **3** (2), 026003 (13pp), (2008).
159. K. G. Götz, Optomotorische untersuchengen des visuellen systems einiger augnmuntanten der fruchfliege drosophila, *Kybernetik*. **2**, 77–92, (1964).
160. G. Westheimer, *Visual hyperacuity*. (Ottoson, Sensory Physiology 1, Springer, Berlin, 1981).
161. P. N. Prokopowicz and P. R. Cooper, The dynamic retina: Contrast and motion detection for active vision, *International Journal of Computer Vision*. **16**, 191–204, (1995). ISSN 0920-5691. 10.1007/BF01539626.
162. S. Ando, T. Nakamura, and T. Sakaguchi. Ultrafast correlation image sensor: concept, design, and applications. In *Proc. International Conference on Solid State Sensors and Actuators TRANSDUCERS '97 Chicago*, vol. 1, pp. 307–310 (16–19 June, 1997). doi: 10.1109/SENSOR.1997.613645.
163. E. M. Yeatman, P. J. Kushner, and D. A. Roberts, Use of scanned detection in optical position encoders, *IEEE J Instrument.and Measur.* **53**(1), 37–44, (2004). doi: 10.1109/TIM.2003.821502.
164. L. Wei, D. Levi, R. Li, and S. Klein, Feasibility study on a hyperacuity device with motion uncertainty: Two-point stimuli, *Systems, Man, and Cybernetics, Part B: Cybernetics, IEEE Transactions on*. **37**(2), 385 –397 (april, 2007). ISSN 1083-4419. doi: 10.1109/TSMCB.2006.883871.
165. S. Zozor, P.-O. Amblard, and C. Duchêne, Does eye tremor provide the hyperacuity phenomenon?, *Journal of Statistical Mechanics: Theory and Experiment*. **2009**(01), P01015, (2009).
166. A. Brückner, J. Duparré, A. Bräuer, and A. Tünnermann, Artificial compound eye applying hyperacuity, *Opt. Express*. **14**(25), 12076–12084, (2006).
167. J. Benson, G. Luke, C. Wright, and S. Barrett. Pre-blurred spatial sampling can lead to hyperacuity. In *Digital Signal Processing Workshop and 5th IEEE Signal Processing Education Workshop, 2009. DSP/SPE 2009. IEEE 13th*, pp. 570 –575 (jan., 2009). doi: 10.1109/DSP.2009.4785988.
168. G. Luke, C. Wright, and S. Barrett, A multiaperture bioinspired sensor with hyperacuity, *Sensors Journal, IEEE*. **12**(2), 308 –314 (feb., 2012). ISSN 1530-437X. doi: 10.1109/JSEN.2010.2099112.
169. F. A. Miles, The neural processing of 3-d visual information: evidence from eye movements., *Eur J Neurosci*. **10**(3), 811–822 (Mar, 1998).
170. S. Tabak and H. Collewijn, Human vestibulo-ocular responses to rapid, helmet-driven head movements., *Exp Brain Res*. **102**(2), 367–378, (1994).
171. G. B. Gauthier, J. P. Piron, J. P. Roll, E. Marchetti, and B. Martin, High-frequency vestibulo-ocular reflex activation through forced head rotation in man., *Aviat Space Environ Med*. **55**(1), 1–7 (Jan, 1984).
172. E. F. Maas, W. P. Huebner, S. H. Seidman, and R. J. Leigh, Behavior of human horizontal vestibulo-ocular reflex in response to high-acceleration stimuli., *Brain Res.* **499**(1), 153–156 (Oct, 1989).
173. R. Hengstenberg, Biological sensors. controlling the fly's gyroscopes., *Nature*. **392** (6678), 757–758 (Apr, 1998). doi: 10.1038/33796.
174. J. Zeil, N. Boeddeker, and J. M. Hemmi, Vision and the organization of behaviour., *Curr Biol*. **18**(8), R320–R323 (Apr, 2008). doi: 10.1016/j.cub.2008.02.017.
175. G. Katzir, E. Schechtman, N. Carmi, and D. Weihs, Head stabilization in herons., *J Comp Physiol [A]*. **187**(6), 423–432 (Jul, 2001).
176. A. Garm, M. O'Connor, L. Parkefelt, and D.-E. Nilsson, Visually guided obstacle avoidance in the box jellyfish tripedalia cystophora and chiropsella bronzie., *J Exp*

Biol. **210**(Pt 20), 3616–3623 (Oct, 2007). doi: 10.1242/jeb.004044.
177. S. Viollet, L. Kerhuel, and N. Franceschini. A 1-gram dual sensorless speed governor for micro-air vehicles. In *Control and Automation, 2008 16th Mediterranean Conference on*, pp. 1270–1275 (25-27 June, 2008). doi: 10.1109/MED.2008.4602072.
178. R. M. Steinman, Voluntary control of microsaccades during maintained monocular fixation, *Sciences.* **155**, 1577–1579, (1967).
179. W. Becker, *Vision and visual dysfunction (Vol 8)*, chapter 5 : Saccades, pp. 95–137. GR.H.S. Carpenter (Ed) Macmillan Press, Ltd, (1991).
180. L. Kerhuel, S. Viollet, and N. Franceschini. A sighted aerial robot with fast gaze and heading stabilization. In *Intelligent Robots and Systems, 2007. IROS 2007. IEEE/RSJ International Conference on*, pp. 2634–2641 (Oct. 29 2007-Nov. 2, 2007). doi: 10.1109/IROS.2007.4399497.
181. B. M. Chen, T. H. Lee, K. Peng, and V. Venkataramanan, *Hard Disk Drive Servo Systems 2nd Edition.* (Springer, Berlin, 2006).
182. R. H. S. Carpenter, *Movements of the eyes, 2nd edt.*, chapter 2 : Vestibular eye movements. PION, London, (1988).
183. B. Lurie and P. Enright, *Classical feedback control with Matlab.* Control Engineering, (Marcel Dekker, 2000).